AD-A266 873

‖‖‖‖‖‖‖‖‖‖‖‖‖‖‖‖‖‖

SEISMIC EVENT LOCATION AT REGIONAL AND TELESEISMIC DISTANCES

C. H. Thurber
H. R. Quin

University of Wisconsin System
750 University Avenue
Madison, WI 53706

31 December 1992

DTIC
ELECTE
JUN 22 1993
S E D

PHILLIPS LABORATORY
Directorate of Geophysics
AIR FORCE MATERIEL COMMAND
HANSCOM AIR FORCE BASE, MA 01731-5000

93-13912

‖‖‖‖‖‖‖‖‖‖‖‖‖‖
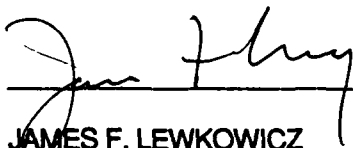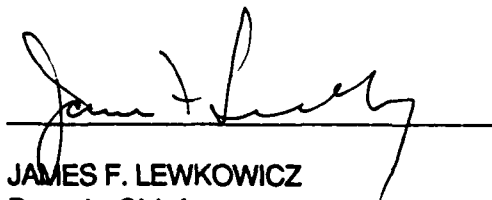
93 6 21 018

The views and conclusions contained in this document are those of the authors and should not be interpreted as representing the official policies, either expressed or implied, of the Air Force or the U.S. Government.

This technical report has been reviewed and is approved for publication.

JAMES F. LEWKOWICZ
Contract Manager
Solid Earth Geophysics Branch
Earth Sciences Division

JAMES F. LEWKOWICZ
Branch Chief
Solid Earth Geophysics Branch
Earth Sciencs Division

DONALD H. ECKHARDT, Director
Earth Sciences Division

REPORT DOCUMENTATION PAGE

Public reporting burden for this collection of information is estimated to average 1 hour per response, including the time for reviewing instructions, searching existing data sources, gathering and maintaining the data needed, and completing and reviewing the collection of information. Send comments regarding this burden estimate or any other aspect of this collection of information, including suggestions for reducing this burden, to Washington Headquarters Services, Directorate for Information Operations and Reports, 1215 Jefferson Davis Highway, Suite 1204, Arlington, VA 22202-4302, and to the Office of Management and Budget, Paperwork Reduction Project (0704-0188), Washington, DC 20503

1. AGENCY USE ONLY (Leave blank)	2. REPORT DATE 31 December 1992	3. REPORT TYPE AND DATES COVERED Final, 8/21/90-12/31/92

4. TITLE AND SUBTITLE	5. FUNDING NUMBERS
Seismic Event Location at Regional and Teleseismic Distances	F19628-90-K-0047 PE 62101F
6. AUTHOR(S) C. H. Thurber and H. R. Quin	PR 7600 TA 09 WU BG

7. PERFORMING ORGANIZATION NAME(S) AND ADDRESS(ES)	8. PERFORMING ORGANIZATION REPORT NUMBER
Board of Regents of the University of Wisconsin System 750 University Avenue Madison, WI 53706	144-BW33-Final

9. SPONSORING/MONITORING AGENCY NAME(S) AND ADDRESS(ES)	10. SPONSORING/MONITORING AGENCY REPORT NUMBER
Phillips Laboratory Hanscom AFB, MA 01731-5000 Contract Manager: James Lewkowicz/GPEH	PL-TR-92-2304

11. SUPPLEMENTARY NOTES

12a. DISTRIBUTION/AVAILABILITY STATEMENT	12b. DISTRIBUTION CODE
Approved for public release; Distribution unlimited	

13. ABSTRACT (Maximum 200 words)

3-component data from Kazakhstan events were analyzed to model the structure and examine the use of secondary phases in event location. Including PmP decreases focal depth uncertainty. All but one of the events are concluded to be explosions; the remaining event is uncertain. Using this structure for the source region, we model nuclear explosions at KTS recorded at 4 stations in the distance range 600-1000 km using a modification of the generalized ray method with separate source and receiver structures. We match first arrivals within about 0.3 seconds, secondary phases within about a second, and obtain good fits to the waveform envelopes.

Locations of nuclear explosions from 1987 to 1989 at Balapan, KTS, were derived with a precision of about 100 m from time-sequence satellite images and teleseismic epicenter estimates. Ground control points for rectification were obtained from information on explosions in Bocharov et al. (1989). Fresh disturbances in satellite images are associated with individual explosions. The seismic locations have error estimates that are too small: in 80% of cases, events lie outside the error ellipses. Our effort was extended to the analysis of LANDSAT images. We have identified nearly all explosion sites from 1973 through 1985.

14. SUBJECT TERMS			15. NUMBER OF PAGES 68
Kazakhstan, crustal structure, synthetic seismograms, regional seismic waves, event location, satellite images			16. PRICE CODE

17. SECURITY CLASSIFICATION OF REPORT	18. SECURITY CLASSIFICATION OF THIS PAGE	19. SECURITY CLASSIFICATION OF ABSTRACT	20. LIMITATION OF ABSTRACT
UNCLASSIFIED	UNCLASSIFIED	UNCLASSIFIED	SAR

TABLE OF CONTENTS

PAGE

1. Summary

Our efforts during the project were divided among two components of study: (1) regional waveform modeling and hypocenter determination and (2) joint satellite image and teleseismic location analysis. Results from each component of our research are summarized below.

Three component seismic data from a set of presumed explosions recorded by stations at Bayanaul and Karkaralinsk in Kazakhstan were analyzed in order to model the crustal structure of the region and to examine the use of the arrival times of secondary P phases in regional event location. Data from the first 5 to 10 seconds of 13 presumed explosions were modeled with the reflectivity method. A good fit to the arrival times and amplitudes in the first five seconds of the P wave was obtained in the epicentral distance range of 100 to 300 km. The crustal P wave velocity model we derived has an upper crustal velocity increasing fairly rapidly from 4.5 km/sec near the surface to 6.5 km/sec at 15 km depth, then increasing more slowly to 7.05 km/sec at 50 km depth. We used the derived crustal model and the primary and secondary P wave arrival times to relocate events in the Kazakhstan region. Inclusion of the phase PmP substantially decreases the focal depth uncertainty for many events. All but one of the events analyzed are concluded to be surface explosions; the identity of the remaining event is uncertain.

Using this velocity model for the source region, we extended our analysis to greater distances. Waveforms from nuclear explosions at the Kazakhstan test site in the years 1971-1989 recorded at four stations in the distance range 600-1000 km were modeled using a modified version of the generalized ray Cagniard code that includes separate source and receiver velocity structures to account for the effect of lateral heterogeneity. We obtained separate receiver models for each station region with the source region model obtained above. We match the observed first arrival within about 0.3 seconds by varying the crust and upper mantle structure at the receiver. The secondary phases from the upper mantle are matched within about 1 or 2 seconds in the first 10 seconds after the first arrival, and we also obtain good fits to the overall waveform envelopes.

Locations of 20 nuclear explosions from 1987 to 1989 at the Balapan test site in Kazakhstan were derived with a precision of about 100 m from a combination of time-sequence satellite images and teleseismic epicenter estimates. Ground control points for satellite image rectification were obtained from information on Balapan explosions published by Bocharov et al. (1989). Fresh disturbances mapped in rectified SPOT satellite images have been associated with individual explosions. The seismically-determined locations are associated with formal error estimates (95% confidence ellipses) that are significantly too small. In 15 out of 19 cases, the events are found from satellite imagery to lie outside these ellipses. Our effort was then extended to the analysis of older LANDSAT images. We have been successful in identifying nearly all events from 1973 through 1985.

2. Accomplishments

2.1. Task Objectives

The goal of this project has been to address some of the difficulties faced in regional and teleseismic event location for seismic verification purposes. The data we have analyzed include near-regional and far-regional seismograms, teleseismic arrival times, and satellite images.

For regional event location, we have been concerned with the effect of source distance, source depth, and regional velocity structure on the initial P waveform (about 10 seconds following first-P). At near-regional distances (less than about 500 km), a single plane-layered velocity structure tends to be adequate for waveform modeling. In this distance range, distinct secondary P phases often can be observed and identified, and hence can provide valuable constraint on source location and depth. The data we have analyzed are from the former NRDC/Soviet Academy of Sciences network in Kazakhstan. Our objective has been to confirm the identity of secondary phases via waveform modeling, improving the model of velocity structure in the vicinity of the Kazakhstan Test Site (KTS) in the process, and evaluating the contribution of secondary phases to event location capability (see section 2.4.1). At mid- to far-regional distances (500 to 2000 km), a single plane-layered velocity structure is generally no longer adequate for waveform modeling, and secondary P phases are more difficult to identify. Our objectives have been to adapt the generalized ray seismogram synthesis technique to incorporate separate source and receiver structures, and use this method to model regional P waveforms and velocity structure in Central Asia, using sources from KTS and vicinity (see section 2.4.2). Using this modeling capability, we begin to address the question of depth determination for seismic events recorded at moderate regional distances based on initial P waveform characteristics.

For teleseismic location, our basic objective is to establish a framework for evaluation of teleseismic location capability by deriving "ground truth" information for the majority of nuclear explosions with $m_b > 5$ at the Balapan (Shagan River) area of KTS. Initially, our efforts involved the use of SPOT images for recent (1987 to 1989) nuclear explosions Firm identification was made of the sites of 18 of the 20 events from this period, plus provisional identification of the remaining 2 (see section 2.4.3). We then turned our attention to LANDSAT images covering the time period 1974 to 1982. Despite the lower resolution of the LANDSAT data (80 m, versus 10 or 20 m for SPOT), we again succeeded in firmly identifying the vast majority of the sites of nuclear explosions in this period, and using the 1982 LANDSAT and 1986 SPOT images, nearly all of the event sites between 1982 and 1986 (see section 2.4.4). With this identification effort completed to the extent possible, these "ground truth" results can be put to future use for a variety of purposes.

2

2.2. Technical Problem

Seismic event location remains a fundamental component of monitoring efforts related to verifying nuclear test ban or test limitation treaties. Event location, especially depth determination, is important both as a basis for discrimination and as a starting point for the analysis of wave propagation and attenuation. The earthquake location problem is relatively well understood on a theoretical basis. However, it can be expected that event location will be a non-trivial problem for in-country regional networks and global non-proliferation monitoring. The following paragraphs are adapted from the contribution of the PI to DARPA's Seismic Identification Workshop report.

Considerable progress has been achieved on the problem of epicenter determination for small events at regional distances with sparse networks and/or arrays. One of the keys to improved results is the incorporation of arrival azimuth and slowness information in the location procedure. A number of recent studies have demonstrated the capability for epicenter accuracy of a few tens of kilometers at regional distances. It is also apparent that location accuracy can be improved if information is available on crust and mantle structure between the sources and receivers , as well as arrival azimuth anomalies at the receivers. Thus there is a need to develop and apply methods for calibrating velocity structure in (possibly remote) source regions and evaluating near-receiver wave propagation anomalies. Travel time and azimuth uncertainties must be reduced substantially in order to achieve a level of location accuracy (10 to 20 km) that would permit identification of potential surface sources of seismic events in satellite imagery.

The problem of depth determination has proven to be much more difficult than epicenter determination. At short distances (< 500 km), Rg excitation is often diagnostic of near-surface sources, but Rg does not usually propagate to large distance. At near-regional distances (500 to 1000 km), empirical and theoretical works indicate that reasonable depth constraint ($\pm$ 5 km) can be obtained if arrival times of secondary phases (Pg, Sn, Lg) are available and lithospheric structure is accurately known. However, at far-regional distances (1000 to 2000 km), the combination of lateral heterogeneity, crustal attenuation, and crustal reverberation is likely to prevent routine use of secondary phase times other than Lg, which has the greatest timing (and modeling) uncertainty. Instead, modeling of body-wave depth phases (pP, sP, etc.) would appear to be necessary. Depth phases are often detected reliably by arrays, but methods to identify them from sets of single-station recordings are needed. The goal in depth estimation should be an ability to determine with 90% certainty whether or not a particular event occurred within 1 kilometer of the surface.

Progress in epicenter and depth determination will require both theoretical and empirical investigations, the latter based on data for which "ground truth" is available. The limitations of existing and new approaches need to be determined for appropriate nonproliferation scenarios. In particular, it is critical to know how much additional information might be required for successful location and depth determination of suspicious events in new (previously uncalibrated) regions.

3

2.3. General Methodology

Our methodology for this project involves 3 primary elements: (1) regional seismic waveform modeling; (2) teleseismic joint epicenter determination, and (3) satellite image analysis.

Three component seismic data from a set of presumed explosions recorded by stations at Bayanaul and Karkaralinsk in Kazakhstan were analyzed in order to model the crustal structure of the region and to examine the use of the arrival times of secondary P phases in regional event location. Data from the first 5 to 10 seconds of 13 presumed explosions were modeled with the reflectivity method, and a new regional velocity structure was obtained. Using this velocity model for the source region, we extended our analysis to stations at greater distances. Waveforms from nuclear explosions at the Kazakhstan test site in the years 1971 to 1989 recorded at four stations in the distance range 600 to 1000 km were modeled using a modified version of the generalized ray Cagniard code that includes separate source and receiver velocity structures to account for the effect of lateral heterogeneity. We obtained separate receiver models for each station region with the source region model obtained above.

For our teleseismic location efforts, we utilized the algorithms JED and MLOC for joint epicenter determination. We examined the sensitivity of the locations to the use of single or multiple master events. Our goal was to establish an estimate of the level of uncertainty that might be associated with these location estimates, so that this uncertainty would be taken into account when time-sequence satellite images were subsequently analyzed.

Ground control points for SPOT satellite image rectification were obtained from information on Balapan explosions published by Bocharov et al. (1989). Locations of 20 nuclear explosions from 1987 to 1989 at the Balapan test site in Kazakhstan were derived with a precision of about 100 m from a combination of time-sequence SPOT satellite images and teleseismic epicenter estimates. Our effort was then extended to the analysis of older LANDSAT images. Enhancement techniques were evaluated in order to maximize the visibility of shot point features.

2.4. Technical Results

The project duration was approximately 28 months, 8/21/90 to 12/31/92. Our efforts during the period were divided among two components of study: (1) regional waveform modeling and hypocenter determination and (2) joint satellite image and teleseismic location analysis. Progress achieved in these two project components is described in the following four subsections.

2.4.1. Seismic velocity structure and event relocation in Kazakhstan from secondary P phases

4

SEISMIC VELOCITY STRUCTURE AND EVENT RELOCATION IN KAZAKHSTAN FROM SECONDARY P PHASES

By H. R. Quin and C. H. Thurber

Abstract

Three-component seismic data from a set of presumed explosions recorded by stations at Bayanaul and Karkaralinsk in Kazakhstan were analyzed in order to model the crustal structure of the region and to examine the use of the arrival times of secondary P phases, primarily PmP, in regional event location. Polarization analysis aided in the identification of the secondary phases. Low-pass filtered data (4-Hz corner) from the first 5 to 10 sec of 13 presumed explosions were modeled with the reflectivity method. The two chemical explosions in 1987 provided a check on accuracy, as their locations and origin times are accurately known. A good fit to the arrival times and amplitudes in the first 5 sec of the P wave (Pn, Pg, and PmP) was obtained in the epicentral distance range of 100 to 300 km. Beyond 300 km, the simple layered model was not adequate to model the PmP arrival.

The crustal P-wave velocity model we derived has an upper crustal velocity increasing fairly rapidly from 4.5 km/sec near the surface to 6.5 km/sec at 15-km depth, then increasing more slowly to 7.05 km/sec at 50-km depth. The observed difference in the arrival times of the phases Pg, PmP, and Pn in the range between 100- and 250-km distance required a relatively sharp transition at the crust mantle boundary. The model is generally similar to previous estimates of P velocity structure in the region, though with a gentler gradient in the upper crust and a steeper gradient in the lower crust. We used the derived crustal model and the primary and secondary P-wave arrival times to relocate events in the Kazakhstan region. Inclusion of the phase PmP substantially decreases the focal depth uncertainty for many of the events. All but one of the events analyzed are concluded to be surface explosions; the identity of the remaining event is uncertain.

Introduction

Seismic event location at regional distances has traditionally relied on P-wave first arrivals at a large number of stations. However, in the case of a sparse regional network or regional arrays, event location often must be done by incorporating seismic wave azimuths and/or timing of both first and secondary arrivals. Previous work on near-regional data from Kazakhstan (Thurber *et al.*, 1989; Li and Thurber, 1991) indicates that secondary P phases can be observed in many seismograms. Secondary P phases have been modeled in many studies in other areas (e.g., Helmberger and Engen, 1980; Langston, 1982; Holt and Wallace, 1989; Vogfjord and Langston, 1991), especially long-period P_{nl}, but to our knowledge these phases have not been used for regional event location studies except for Thurber *et al.* (1989) and Li and Thurber (1991). We have undertaken a study to determine whether or not secondary phases can be accurately identified, using a combination of polarization analysis and seismogram synthesis, and then utilized to improve event locations.

This study is motivated by a number of factors. One direct goal is to test the conclusions of Li and Thurber (1991) regarding the utility of *PmP* for improving

2494

near-regional event location with a sparse network, particularly in terms of constraining source depth. The need for improving regional event location capability is likely to increase as concerns regarding nuclear weapons proliferation grow. A related goal is to reevaluate the events in Kazakhstan studied by Thurber *et al.* (1989) to confirm the presumption that they are surface explosions. A third goal is to provide a source-region velocity model for future studies of far-regional and teleseismic waves from Kazakhstan nuclear explosions.

We study the regional phases Pg, Pn, and PmP from a set of 13 events recorded by the Natural Resources Defense Council/Soviet Academy of Sciences (NRDC/SAS) network in the Kazakhstan region that operated in the years 1987 to 1988 (Fig. 1). The network stations, consisting of 3 sets of three-component seismometers, produced about two dozen high-quality multi-station recordings of explosions in the epicentral distance range 25 to 450 km (Thurber *et al.*, 1989). Our analysis focuses on data from stations Bayanaul (BAY) and Karkaralinsk (KKL), as station Karasu (KSU) suffered from a serious site effect (Berger *et al.*, 1988) and also was in a region of different velocity structure (Leith, 1987). A number of secondary P phases have been observed on these seismograms that are identified below as either PmP or Pg.
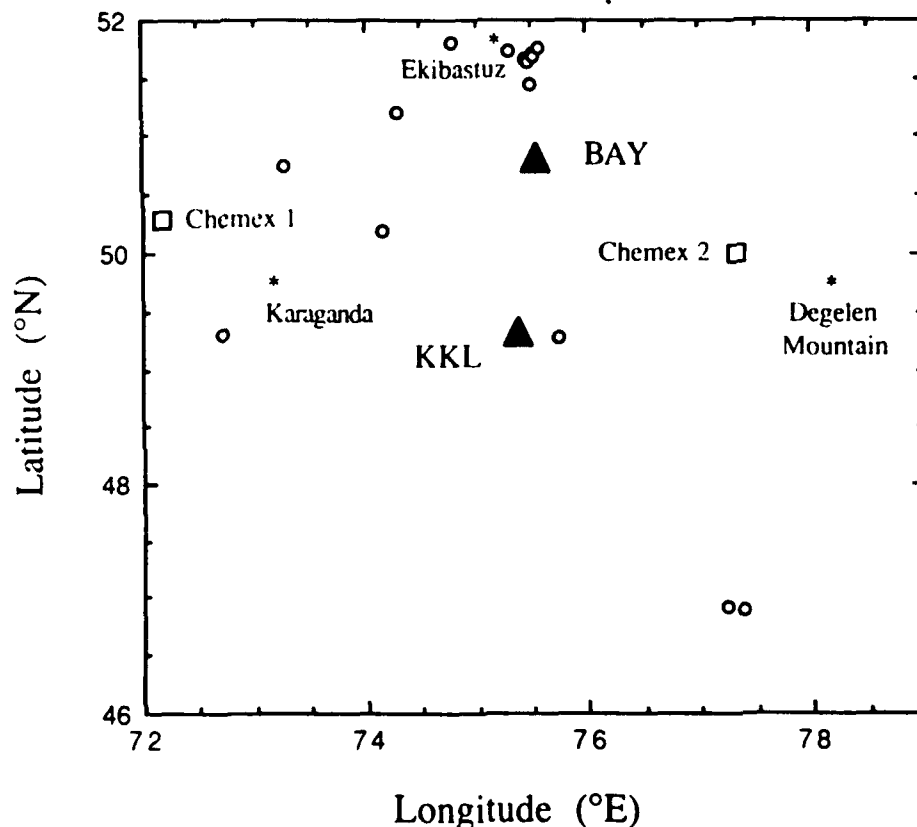

FIG. 1. Map of the Kazakhstan region showing the locations of stations BAY and KKL of the NRDC/SAS network (triangles), 1987 chemical explosions (squares), and the other events analyzed (circles).

PREVIOUS RESEARCH ON CRUSTAL STRUCTURE IN KAZAKHSTAN

An excellent summary of studies of crust and upper mantle structure in Kazakhstan is provided by Ryaboy (1989). This work has shown that the crust in the region has a structure with moderate lateral variations and a crust-mantle boundary depth ranging between 45 and 55 km. Leith (1987) reported a crustal structure obtained from a Deep Seismic Sounding (DSS) profile near the stations KKL and BAY with a 50-km-thick crust and 6 crustal layers, with P velocities increasing monotonically with depth. Priestley et $al.$ (1988) used an inversion of teleseismic P-to-S converted waves at stations BAY and KKL to obtain P velocity models (assuming a constant Vp/Vs value) generally similar to that reported by Leith (1987), except for a slightly decreased crustal thickness at station BAY, a broad Moho transition beneath KKL, and a slight velocity reversal at shallow depths beneath both stations (Fig. 2). Overall, there is evidence for significant lateral crust and upper mantle heterogeneity in this region, though relatively modest heterogeneity in the immediate vicinity of the Kazakhstan Test Site. Therefore, any one-dimensional crustal model is only an approximation to the actual structure in this region. With this limitation in mind, we endeavor to match reflectivity synthetics computed for a simple
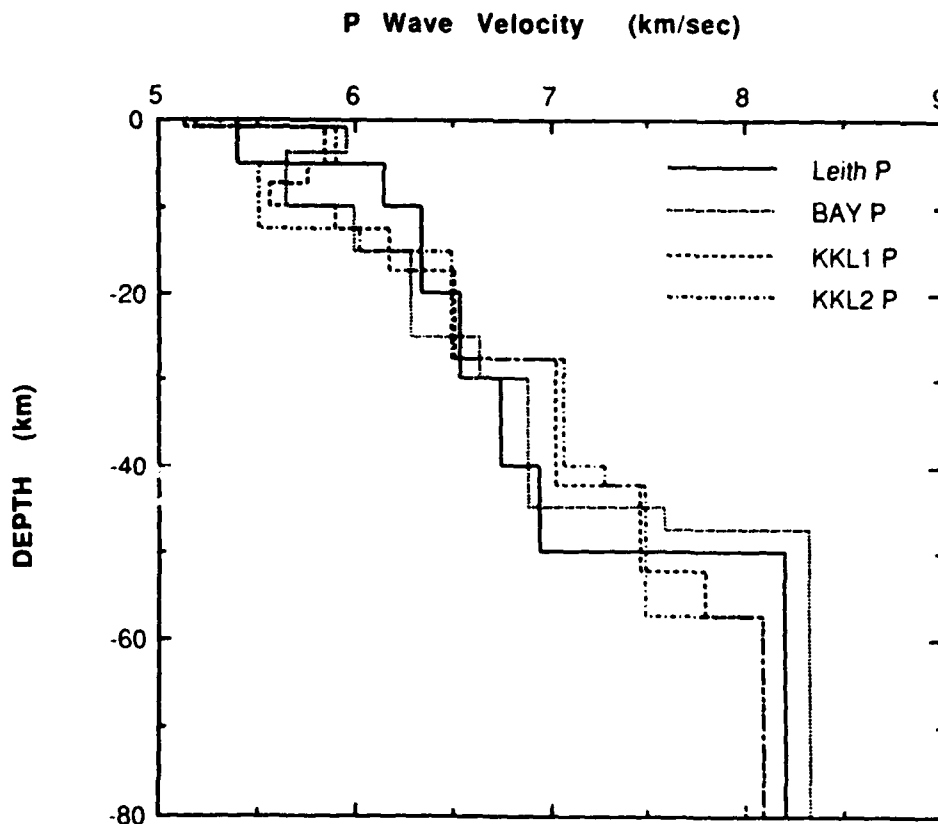

FIG. 2. P-wave velocity models from Leith (1987) from a DSS profile in the Kazakhstan region (solid) and Priestley et $al.$ (1988) from receiver function inversion for stations BAY (dotted) and KKL (two models, dashed and dot-dashed).

one-dimensional crustal model to observed seismic travel times and waveforms. Our main focus is on first and secondary P-wave arrivals and their potential for regional event location.

EXAMINATION OF NEAR-REGIONAL DATA

The data analyzed in this study were recorded on a set of surface mounted Teledyne Geotech GS-13 short-period seismometers, a set of Kinemetrics SV-1 and SH-1 surface-mounted intermediate-period seismometers, and a set of Geotech 54100 borehole-mounted seismometers installed at depths of 66 and 101 m at BAY and KKL, respectively (Berger *et al.*, 1988). The velocity response of each of these instruments (Berger *et al.*, 1988) is flat from at least 1 to 50 Hz. The noise spectrum for these stations is also summarized by Berger *et al.* (1988).

The events used in our analysis have been located by Thurber *et al.* (1989) using body-wave arrival times and P-wave arrival azimuths. Absolute locations are known for the 1987 chemical explosions carried out as part of the NRDC/SAS verification project (Given *et al.*, 1990), other events are clearly associated with mines or quarries observed in satellite images (Thurber *et al.*, 1989), and still others can be associated with mines indicated on regional maps. None of the events used are thought to be earthquakes. There is some uncertainty is the epicentral distances of the events analyzed, so we place special emphasis on those events whose locations are most reliable.

An examination of the unprocessed waveforms at the NRDC/SAS stations BAY and KKL indicates the first P arrival is usually followed by one or more distinct secondary arrivals in the succeeding 0.5 to 2.5 sec in the epicentral distance range between 100 and 300 km (Fig. 3). In the distance range under 100 km from the source, there are no clearly identifiable secondary P arrivals; only the phase Pg can be identified (Fig. 3a). At about 120-km distance from the source, however, the secondary arrival PmP appears about 2.5 sec after the first arrival. The amplitude of this phase relative to the first arrival increases in the distance range from 120 to 170 km from the source, at which point PmP arrives about 2 sec after the first arrival and has about twice the amplitude (Fig. 3b). Between 170 km and the crossover distance of about 240 km, the phases Pg and PmP continue converging and the relative amplitude of PmP generally decreases, until by 300 km distance the two phases are weak and indistinguishable, and we have difficulty picking secondary phases with any reliability (Fig. 3c).

To gain confidence in our identification of these arrivals, we carried out a polarization analysis on the secondary phases to determine whether they had the correct polarization expected for P waves from the event azimuth. The polarization analysis was done using the covariance of the horizontal-component seismograms, as described by Thurber *et al.* (1989). For a polarized signal in the presence of noise, the eigenvector corresponding to the largest eigenvalue of the covariance matrix for the signal components gives the direction of polarization, and the ratio of eigenvalues measures the rectilinearity of particle motion (Kanasewich, 1981). Since we are interested just in the arrival azimuth, the horizontal component seismograms from a station are windowed and demeaned, and the 2-by-2 signal covariance matrix is computed. An example is shown in Figure 4. We find that a large fraction of the presumed secondary arrivals have the same azimuth as the first arrival and show signifi-
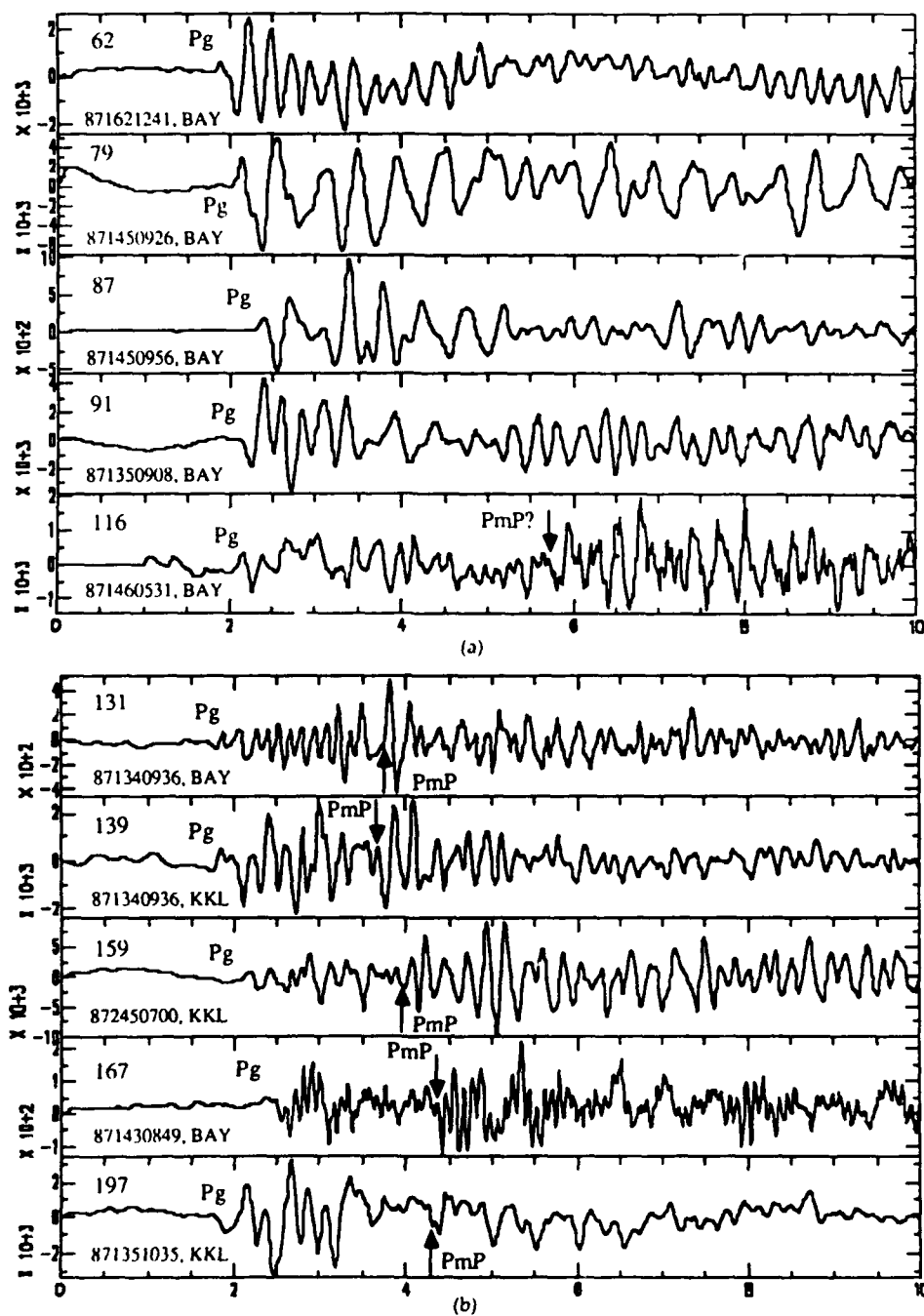
FIG. 3. (a to c) Examples of observed seismograms at a range of epicentral distances. A window of 10 sec is shown beginning about 2 sec before the first P arrival. The epicentral distance is indicated in the upper left of each panel. The phases Pg, Pn, and PmP are indicated.
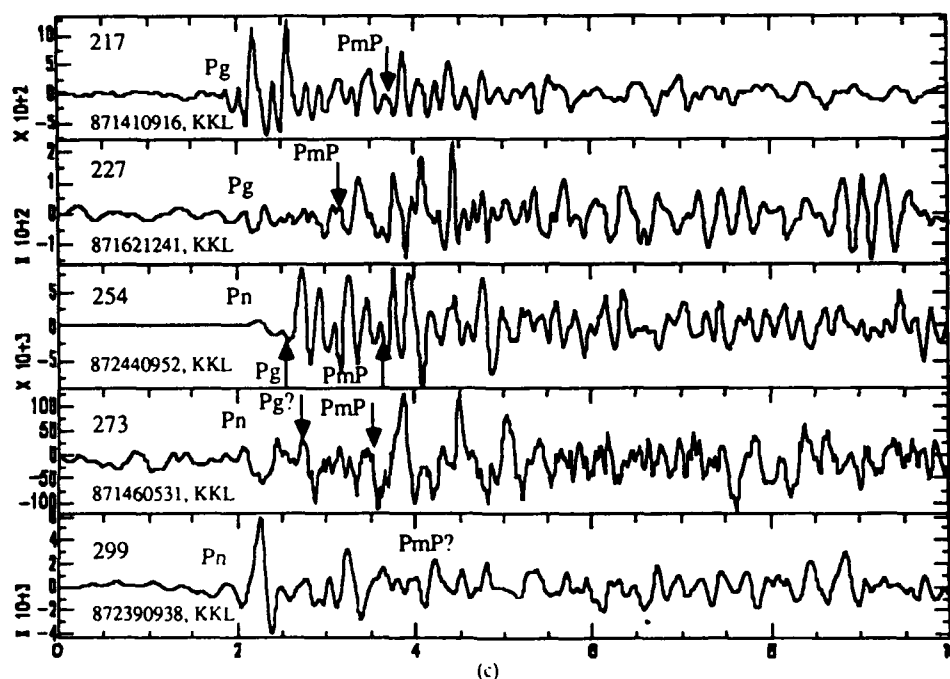
FIG. 3. (Continued).

cant particle motion rectilinearity. When comparing the data to the synthetics, we have considered only the phases that the polarization analysis indicates are from the same azimuth as the first arrival. The polarization analysis and computed arrival times and amplitudes of the synthetic arrivals give us confidence in our ability to pick the secondary phases *Pg* and *PmP*. Consequently, we have confined most of our attention to making reliable picks on these phases, along with *Pn* when it is the first arrival.

CRUSTAL MODEL AND SYNTHETICS

After making initial picks of the phase arrival times, we searched for a crustal model that matched the observed phase arrival times and amplitude ratios. We computed synthetic seismograms using the code of Mallick and Frazer (1987). This code was written for computing high-frequency (up to 20 Hz) synthetic seismograms over regional distances (0 to 1000 km) and a large number of layers. It has been used successfully for a number of different applications, including modeling reflection seismograms in the range 0 to 100 km and modeling high-frequency regional arrivals at distances up to 1400 km (Mallick and Frazer, 1987). For the various models we examine, we compute synthetic seismograms and low-pass filter them using a 4-Hz corner frequency. For comparison with the synthetic seismograms, the observed seismograms were rotated into the azimuth of the source, low-pass filtered with a corner frequency of 4 Hz, and then plotted for 10 sec around the first *P*-wave arrival.

To improve our crustal model, we first computed arrival times of *Pn*, *PmP*, and *Pg* to compare with the data. The crustal models were varied systemati-
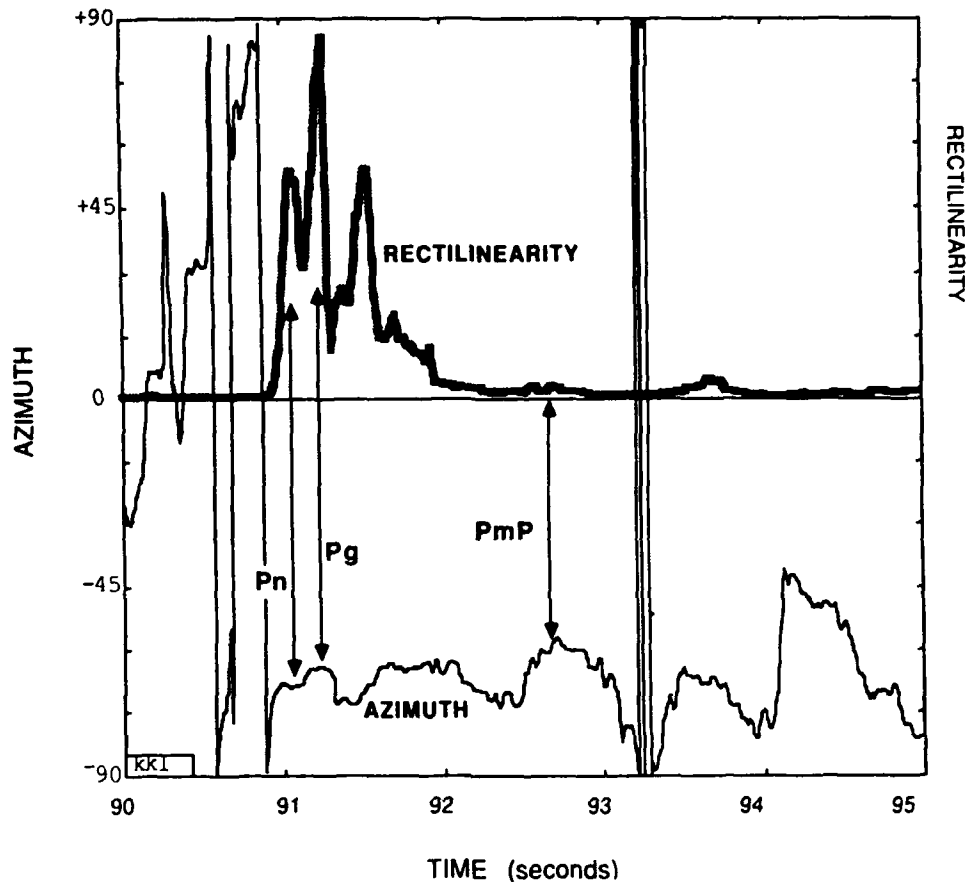
10

FIG. 4. Polarization analysis for 5 sec of an example event showing estimated arrival azimuth (thin solid line) and calculated particle motion rectilinearity (broad shaded line) for the *Pn*, *Pg*, and *PmP* phases. Arrival azimuth ranges are plotted for the range ±90°, while rectilinearity is plotted in the upper portion with an arbitrary scale. This event is the 254 km distance record in Figure 3 (chemex 1, 872450700, at KKL).

cally to see the effects on the synthetic seismograms. We started with the Leith (1987) crustal model and tested variations in the upper- and mid-crustal velocity structure until we obtained good agreement with the *Pg* first arrivals in the distance range less than 100 km from the events. *Pg* and *PmP* arrival times in the distance range 100 to 245 km helped determine the lower crustal velocities. Near the crossover distance of about 240 km, we find considerable waveform complexity in both the data and synthetics. We modeled the *Pn* first arrivals in the distance range between 240 and 300 km to ascertain the transition velocity between 40 and 50-km depth. A transition velocity of 6.95 to 7.05 km/sec was needed in this depth range to model the arrival times of the data. The data require a sharp transition at the crust-mantle boundary at 50-km depth to match the observed difference in the travel times of the different phases. We constrained the upper-mantle velocity in the depth range between 50 and 85 km using the *Pn* arrival times in the distance range between 250 and 350 km. A velocity of 8.25 km/sec in the upper mantle between 55- and 85-km depth gave

the best fit to the arrival time of *Pn* and the observed difference in the arrival times of *Pn* and *PmP* in this distance range. Beyond about 260 km, the largest amplitude secondary arrival has the arrival time expected of *PmP*; however, the synthetic *PmP* considerably exceeds the observed amplitude of *PmP* in the data.

Our final velocity model is presented in Figure 5. It has an upper-crustal velocity increasing fairly rapidly from 4.5 km/sec near the surface to 6.5 km/sec at 15-km depth, then increasing more slowly to 7.05 km/sec at 50-km depth. The crust-mantle transition zone ranges from 8.05 km/sec at 50-km depth to 8.25 km/sec at 55-km depth. The upper mantle has a *P* velocity of about 8.25 km/sec between 55- and 85-km depth. Below this depth, the data do not constrain the velocity structure, and we have used the structure obtained by Goldstein *et al.* (1992). We have assumed a constant value for Vp/Vs of 1.73 throughout the model. Overall, our final model is similar to that obtained from the deep seismic soundings (dashed lines in Fig. 5).

The fit of the data to the synthetics is quite good in the distance range between 100 and 280 km (Fig. 6) and is superior to the Leith model (Fig. 7). This model matches the *Pg*, *PmP*, and *Pn* arrival times within about 0.3 sec for most of the phases seen on the seismograms. We get very good agreement with

VELOCITY (km/sec)

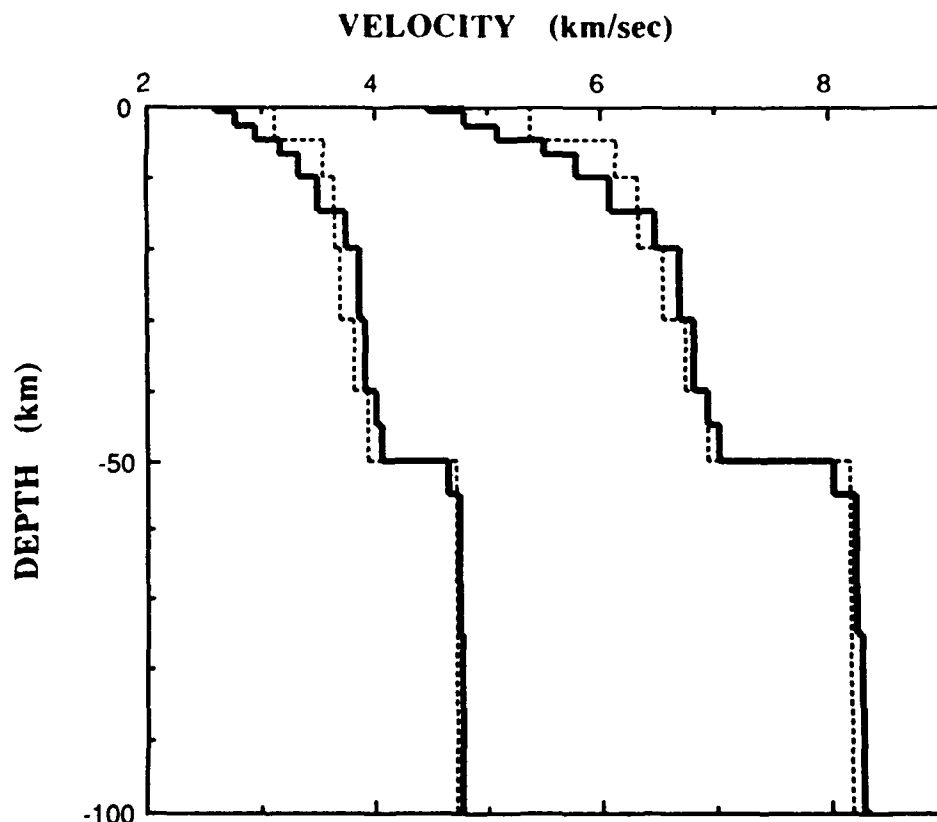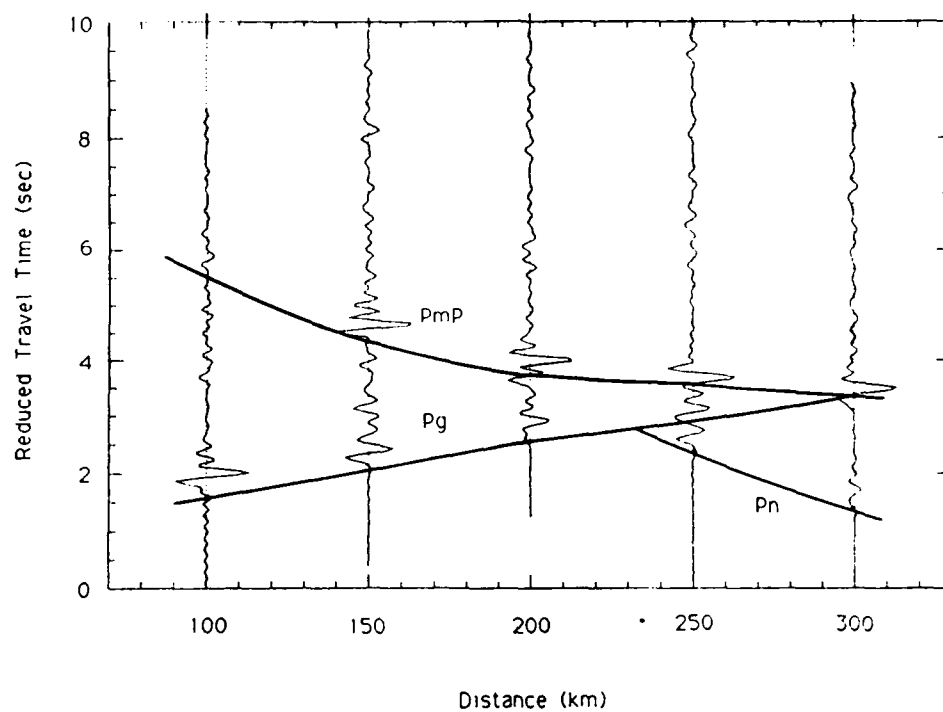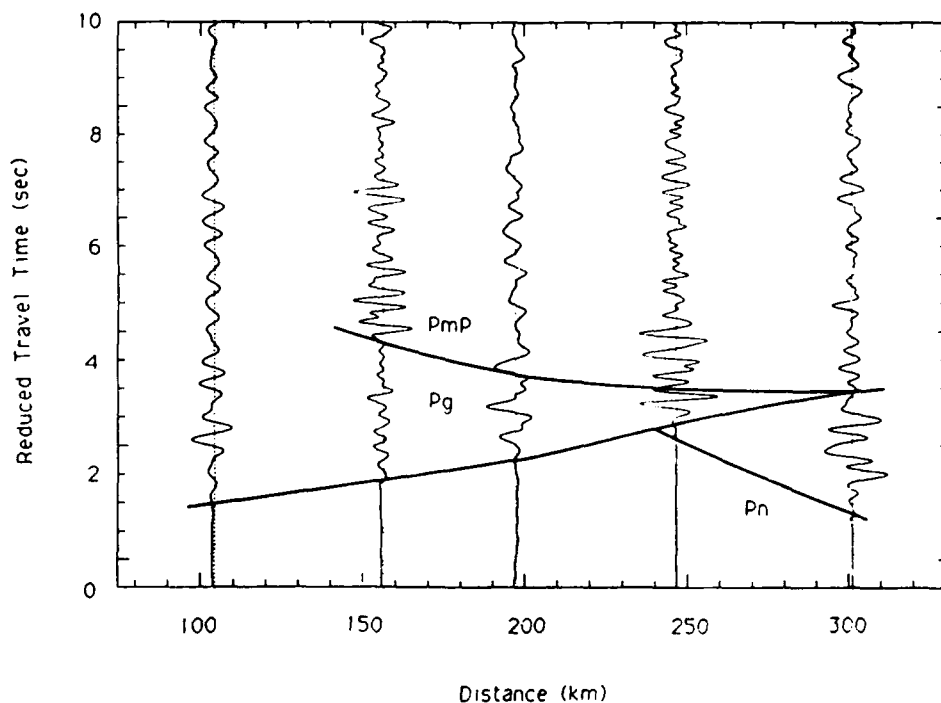FIG. 5. Final velocity structure model for the Kazakhstan region (solid line) compared to the initial model from Leith (1987) (dashed line).

12

FIG. 6. (a and b) Record sections of (a) synthetic seismograms at 100, 150, 200, 250, and 300 km distances and (b) observed data at comparable distances (871460833, 872450927, 871351035, 872450700, and 872440952), using a reducing velocity of 7.5 km/sec.

13

the *Pg* first arrival times in the distance range less than 100 km; however, we find that the initial coda of the data are larger in amplitude than the synthetics. We can attribute this to wave scattering and conversion not modeled by the reflectivity synthetics. Between 100 and 200 km, the first arrival times and the overall waveform envelopes show good agreement; however, the arrival time difference between *Pg* and *PmP* is greater in the synthetics than in the data by between 0.2 and 0.7 sec for the distance range under 150 km, and less in the synthetics than in the data by between 0.3 and 0.9 sec for the distance range beyond 150 km. The model shows the best agreement in the distance range between 180 and 240 km, where the synthetics match both the arrival times and amplitudes of *Pg* and *PmP* within 0.3 sec and 50%, respectively. Near the crossover distance of 240 km, we find that the *Pg*, *Pn*, and *PmP* phases all arrive in the first 1.5 sec of the record on both the synthetic and the data records. Between 250 and 280 km, the synthetic matches the arrival time of *Pn* and *PmP* within 0.3 sec; however, the *Pn* amplitude of the synthetic underestimates that of the data while the synthetic *PmP* amplitude exceeds that of the data, each by about a factor of 2. Beyond 300 km we have difficulty matching the synthetics to the data: every realistic model that matches the *Pn* and *PmP*
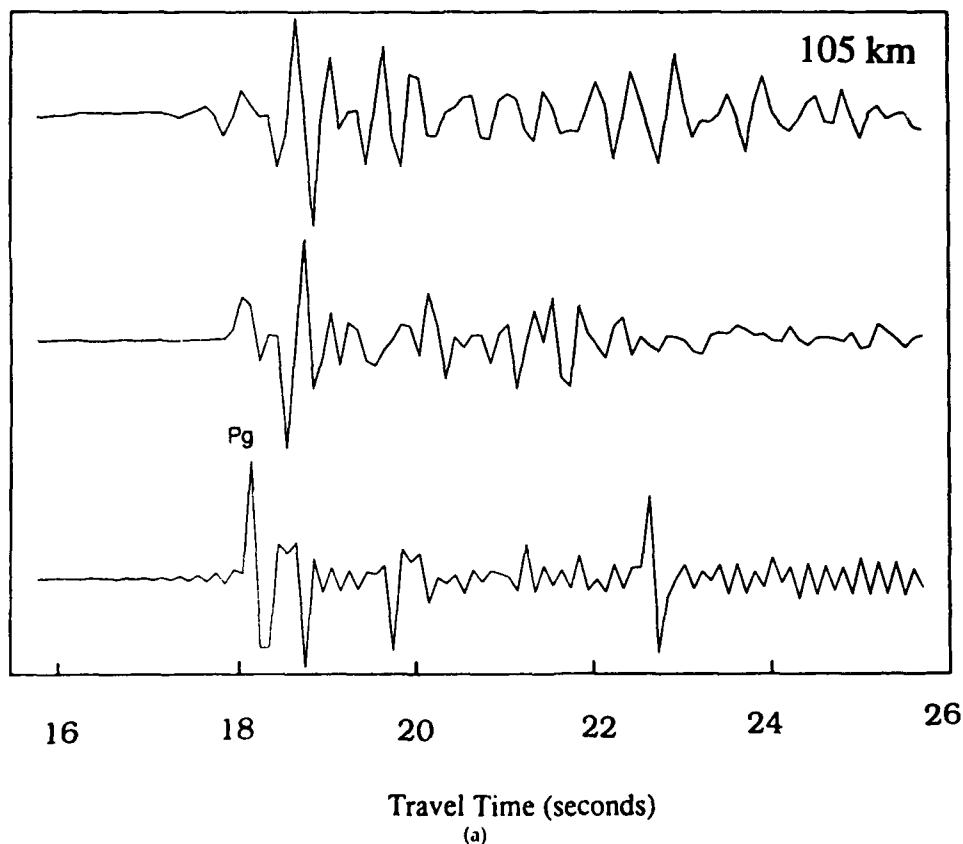

Travel Time (seconds)

(a)

FIG. 7. (a to e) Comparison of observed seismograms (*top*) with reflectivity synthetic seismograms at 105, 156, 197, 257, and 301 km distance for our final model (middle) and the Leith model (*bottom*). The amplitude scale is arbitrary.

14

Travel Time (seconds)

(b)
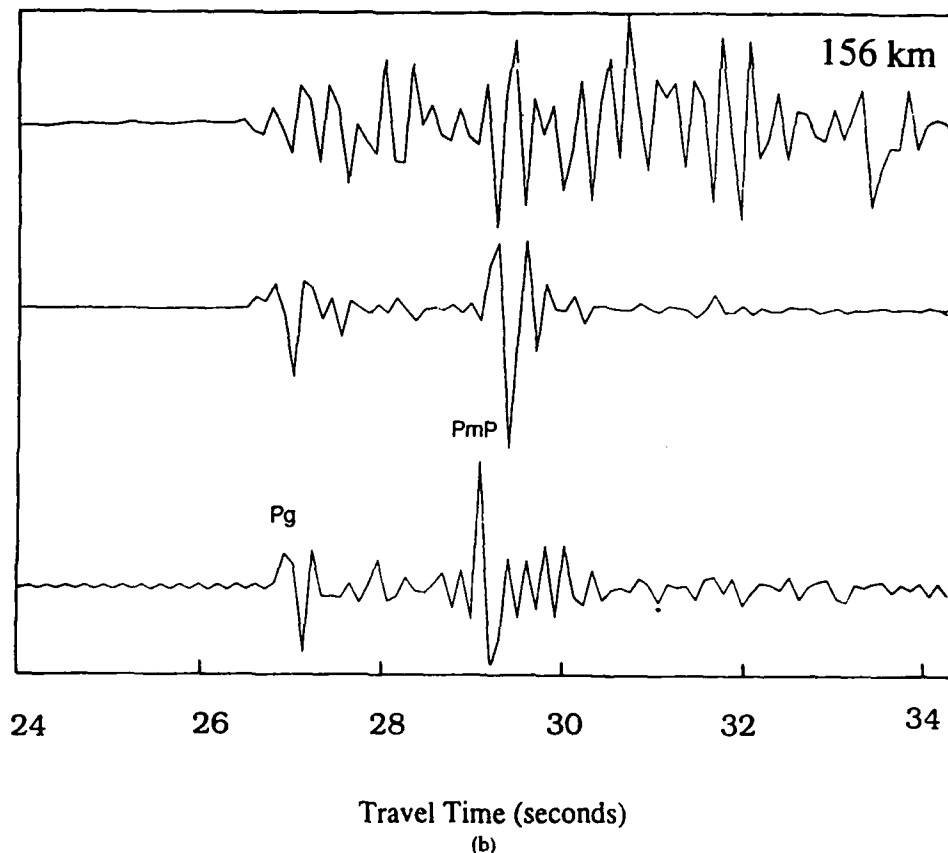
FIG. 7. (Continued).

arrival times in the distance range under 300 km gives a *PmP* amplitude that is a factor of 2 greater than that observed in the data beyond 300 km. We believe that lateral heterogeneity probably renders the assumption of a simple layered model questionable beyond 300 km. Therefore, we believe that using a single-layered crustal model, as required for the reflectivity synthetics, is probably inappropriate for events in the distance range beyond 300 km.

EVENT RELOCATION USING THE PHASES *Pg*, *Pn*, AND *PMP*

Previous empirical and theoretical work on regional event location in Kazakhstan (Thurber *et al.*, 1989; Li and Thurber, 1991) has investigated the usefulness of secondary *P* arrivals for regional event location. With an improved crustal model for Kazakhstan (Fig. 5) and a determination of *Pg* and *PmP* secondary arrivals in the data supported by synthetic seismogram modeling (Figs. 6 and 7), we relocate the regional events in Kazakhstan. Event locations were computed in the same manner as described by Thurber *et al.* (1989), incorporating arrival azimuth information and utilizing the location algorithm TTAZLOC (Bratt and Bache, 1988).

To evaluate the utility of *PmP* for event location, 13 of the events shown in Figure 1 for which *PmP* could be identified were relocated using the new

15

197 km

Pg

PmP

32   34   36   38   40

Travel Time (seconds)

(c)
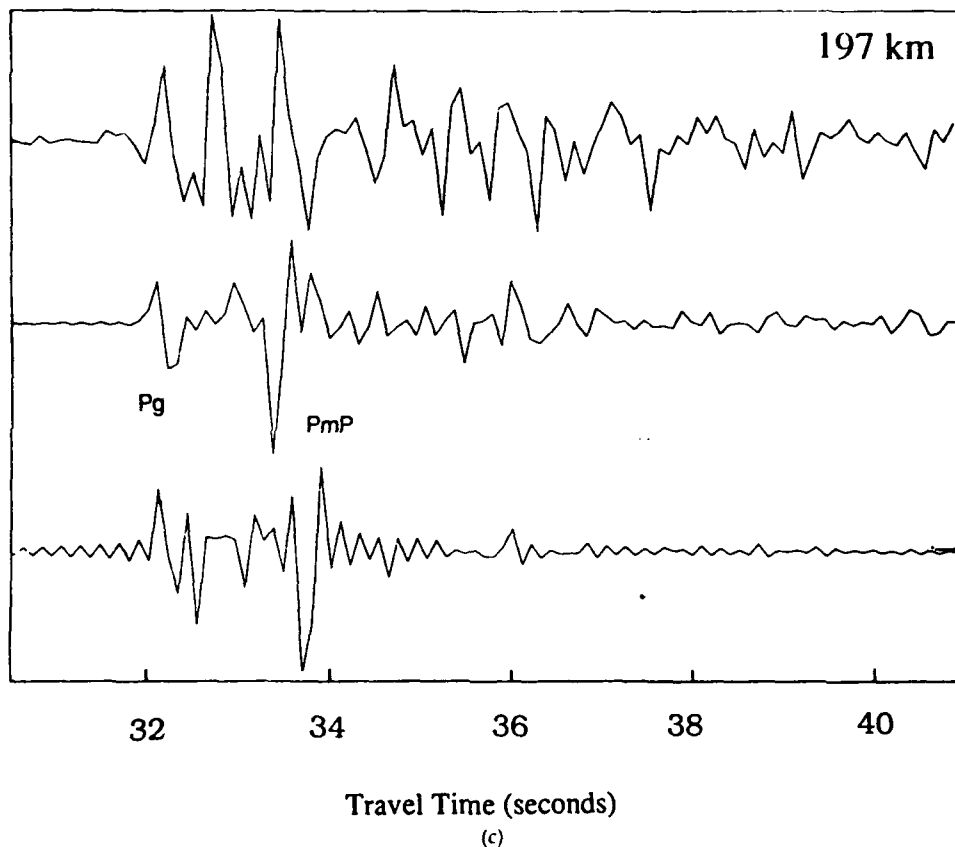
FIG. 7. (*Continued*).

velocity model, both with and without the phase *PmP*. We identified *PmP* on nearly half the seismograms (see Fig. 3 for examples), with estimated reading uncertainties of 0.05 to 0.25 sec. Initally, the events were relocated with focal depth fixed at 0 km, as had been done by Thurber *et al.* (1989) for all but the three chemical explosions (Given *et al.*, 1990). The event locations showed little change, with differences averaging less than 4 km in latitude and 5 km in longitude. The mean RMS residual for all *PmP* observations was about 0.35 sec, compared to 0.25 and 0.50 sec for all *Pn* and *Sn* observations, respectively. Thus, the *PmP* arrival times were of a quality comparable to the previous *Pn* and *Sn* data. The estimated location uncertainties decreased about 10% when *PmP* observations were added, again indicating that the quality of the *PmP* data is comparable to that of the other phases. Most of this decrease can be attributed to the increase number of degrees of freedom due to adding *PmP* without an increase in data misfit.

The theoretical study of Li and Thurber (1991) indicates that *PmP* arrival times can provide significant constraint on source depth for regional events recorded by a sparse network. Therefore, we recomputed the event locations with focal depth unconstrained both with and without the *PmP* observations. The starting value for depth was 0 km, and negative depth values (i.e.,

16
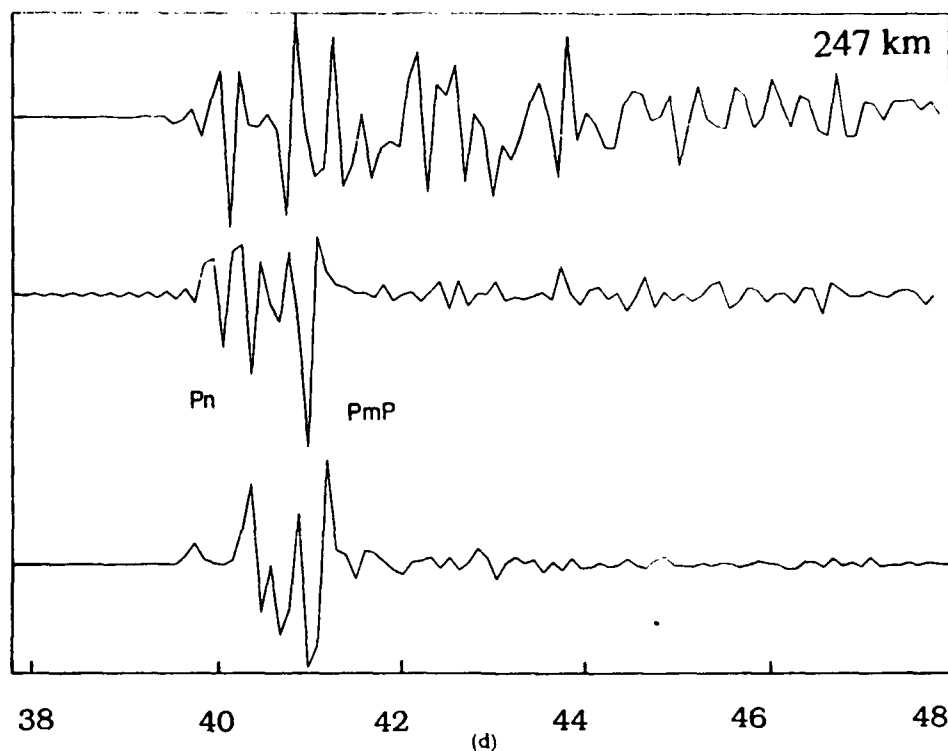
FIG. 7. (Continued).

"airquakes") were prohibited by the algorithm. The RMS residuals from the constrained focal depth location results above were adopted as a priori values for the data variances. As in previous studies (Jordan and Sverdrup, 1981; Bratt and Bache, 1988; Thurber et al., 1989), a priori information was given a K-weight of 8.

The location results with focal depth free are indicated in Table 1. The epicenter locations were again similar with or without PmP; all events had differences in epicenter less than 5 km. Epicentral uncertainties were generally reduced with PmP, but not substantially. The situation for focal depth was quite different, however. Although computed depth differences were not significant, nearly half of the events had their depth uncertainty estimate reduced by a factor of 1.5 or greater when PmP observations were included. Thus, the PmP observations do provide useful constraint on source depths at these near-regional distances.

An important issue implicit in this discussion is the confidence that these events are explosions and not earthquakes. In Table 1, independent information on or associations of these explosions with mines or quarries is indicated. Two of the events are the 1987 chemical explosions, and suspected source areas for seven other events had been identified previously by Thurber et al. (1989) from satellite images (mines at Ekibastuz and Balkash). Of these, events 871351035, 871410916, and 871460833 were also shown to have spectral modulation typical of ripple-fired blasts by Hedlin et al. (1989). In addition, one event (871430849)

Travel Time (seconds)

(e)
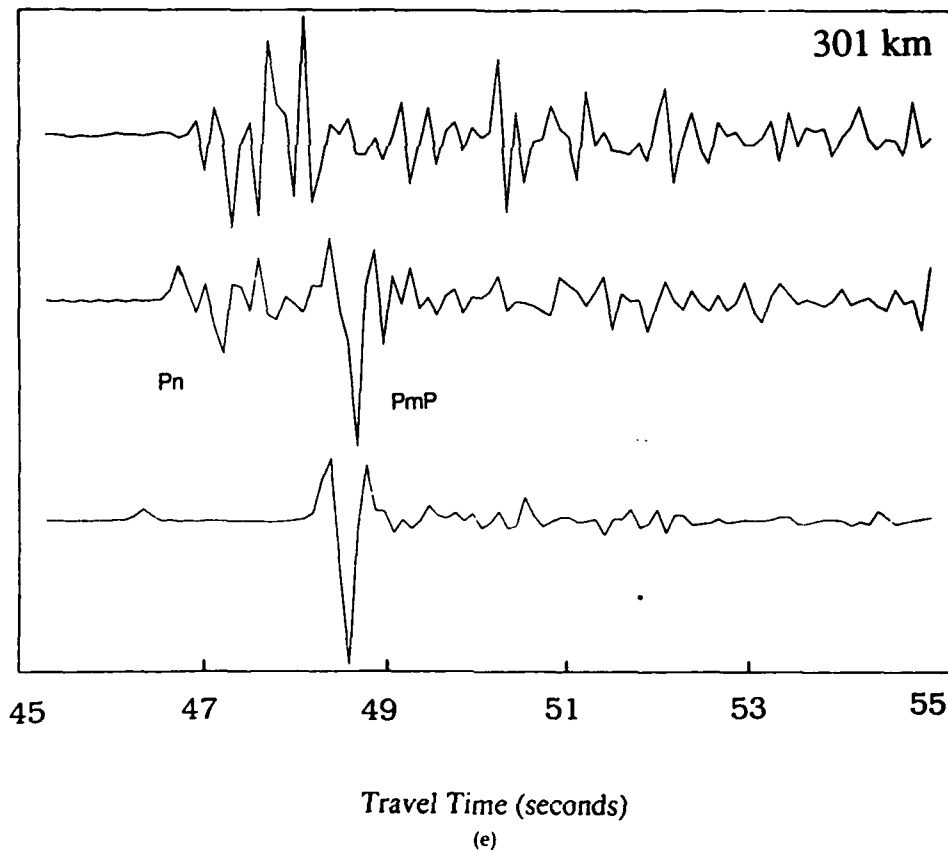
FIG. 7. (Continued).

is thought to have been a blast at a known quarry in the town of Karagayly (H. Given, personal comm.). Of the remaining four events, event 871351035 is located within 4 km of a mapped mine at the town of Yuzhnyy on the 1983 ONC navigational chart for the region, while event 871410916 is located within 10 km of two mapped mines at the town of Molodezhnoye. Of the other two events, 871340936 occurred in the Karaganda area, known for mining, at a time of day typical for mine blasts. Only event 871460531 is "suspicious" due to its time of occurrence, although the location results are not inconsistent with a surface focus.

CONCLUSIONS

Using a reflectivity synthetic seismogram code, we have modeled primary and secondary P phases for a data set from near-regional events recorded in 1987 and 1988 by the stations BAY and KKL of the former NRDC/SAS network. An analysis of wave polarization was used to help identify the secondary phases, primarily PmP. A new layered crustal model for the region was developed to improve the fit to the arrival times and waveforms of these phases. We can match a Pg first arrival and a PmP second arrival on most of the seismograms in the distance range between 100 km and the crossover distance of 240 km

18

TABLE 1

COMPARISON OF EVENT LOCATIONS WITHOUT VERSUS WITH PmP OBSERVATIONS WITH FOCAL DEPTH FREE

Event (yr-day-hr-mn)	Without PmP						With PmP						Association
	Latitude (°N)	Longitude (°E)	Depth (km)	Semi-major axis (km)	Semi-minor axis (km)	Depth axis (km)	Latitude (°N)	Longitude (°E)	Depth (km)	Semi-major axis (km)	Semi-minor axis (km)	Depth axis (km)	
87-134-0936	50.199	73.964	0.0	45.2	10.7	2140.2	50.204	73.958	9.3	39.8	4.7	11.0	Uncertain
87-135-0908	51.804	75.593	0.0	31.8	24.7	12.1	51.793	75.615	0.0	32.9	24.6	11.1	Ekibastuz mine
87-135-1035	49.320	72.886	6.1	14.1	5.4	11.3	49.299	72.873	5.7	10.8	4.7	6.2	Yuzhnyy mine
87-141-0916	50.790	73.214	0.0	65.7	5.1	64.8	50.793	73.251	0.0	12.2	5.4	10.2	Molodezhnoye mine
87-143-0849	49.319	75.689	2.9	11.8	4.5	11.8	49.321	75.699	1.1	9.2	3.9	7.9	Karagayly quary
87-145-0926	51.642	75.545	0.0	24.5	13.0	10.6	51.640	75.549	0.0	23.1	11.5	8.8	Ekibastuz mine
87-145-0956	51.788	75.567	0.0	33.9	15.6	12.7	51.786	75.574	0.0	32.2	14.3	11.3	Ekibastuz mine
87-146-0531	51.950	74.937	0.0	30.5	17.1	13.6	51.949	74.917	0.0	28.7	15.8	12.0	Uncertain
87-146-0833	51.671	75.575	0.0	25.3	12.2	16.0	51.663	75.591	0.0	26.9	12.6	12.4	Ekibastuz mine
87-162-1241	51.379	75.525	0.0	14.2	9.9	16.7	51.368	75.528	0.0	13.4	8.9	8.3	Ekibastuz mine
87-239-0938	46.772	77.354	0.0	83.7	7.9	45.6	46.767	77.351	0.0	59.9	7.3	31.8	Balkash mine
87-245-0700	50.281	72.029	0.0	69.7	6.6	43.6	50.295	71.998	2.6	36.4	6.1	21.9	Chemex 1
87-245-0927	50.018	77.230	0.0	4.9	3.1	8.4	50.011	77.241	0.0	4.4	2.6	6.6	Chemex 2

with an arrival time misfit on the order of 0.5 sec, and the relative amplitudes are also matched within 50%. Beyond the crossover distance, we are able to model *Pn* and *PmP* arrival times with comparable fit, but we have difficulty in matching the observed amplitude of the phase *PmP* beyond 300 km, presumably due to effects of lateral heterogeneity. A secondary *Pg* phase is only observed in the range just beyond the crossover distance.

Our crustal model for the Kazakhstan region has a 4.5 to 6.5 km/sec upper crust (to 15-km depth), a middle and lower crust that increases in velocity from 6.5 to 7.05 km/sec, and a crust-mantle boundary at about 50-km depth. Compared to the model of Leith (1987) derived from DSS studies, our upper crust has a slightly lower velocity and our lower crust has a slightly higher velocity, similar to the results of Priestley *et al.* (1988). A relatively sharp crust-mantle boundary (about 5-km thick) was needed to match the observed difference in the *Pn* and *PmP* arrival times. This is in contrast to the receiver function results of Priestley *et al.* (1988) for the structure beneath station KKL, which suggested a 10- to 15-km-thick transitional Moho. The uppermost mantle has a velocity of 8.05 km/sec between 50- and 55-km depth, increasing to 8.25 km/sec between 55- and 85-km depth. The near-regional data do not constrain the structure at greater depths.

The new velocity structure and *PmP* observations obtained from this study were used to relocate events in the distance range up to about 300 km from the stations. It was found that adding the phase *PmP* reduces the uncertainty for event depth in all cases, with relatively little effect on epicenter uncertainty. None of the events can be conclusively demonstrated to be earthquakes, based on their focal depths and associations with active mines and quarries, though one event cannot be confidently classified as an explosion.

REFERENCES

Berger, J., H. K. Eissler, F. L. Vernon, I. L. Nersesov, M. B. Gokhberg, O. A. Stolyrov, and N. T. Tarasov (1988). Studies of high-frequency seismic noise in eastern Kazakhstan, *Bull. Seism. Soc. Am.* **78**, 1744–1758.

Bratt, S. R. and T. C. Bache (1988). Locating events with a sparse network of regional arrays, *Bull. Seism. Soc. Am.* **78**, 780–798.

Given, H. K., N. T. Tarasov, V. Zhuravlev, F. L. Vernon, J. Berger, and I. L. Nersesov (1990). High-frequency seismic observations in eastern Kazakhstan, USSR, with emphasis on chemical explosion experiments, *J. Geophys. Res.* **95**, 295–307.

Goldstein, P., W. R. Walter, and G. Zandt (1992). Upper mantle structure beneath Central Asia using a source array of nuclear explosions and waveforms at regional distances, *J. Geophys. Res.* **97**, 14097–14113.

Hedlin, M. A. H., J. B. Minster, and J. A. Orcutt (1989). The time-frequency characteristics of quarry blasts and calibration explosions recorded in Kazakhstan, USSR, *Geophys. J. Int.* **99**, 109–121.

Helmberger, D. V. and G. R. Engen (1980). Modeling the long period body waves from shallow earthquakes at regional ranges, *Bull. Seism. Soc. Am* **70**, 1699–1714.

Holt, W. E. and T. C. Wallace (1989). Crustal thickness and upper mantle velocities in the Tibetan

Plateau region from the inversion of Pnl waveforms: evidence for a thick upper mantle lid beneath sourthern Tibet, *J. Geophys. Res.* **95**, 12499-12525.

Jordan, T. H. and K. A. Sverdrup (1981). Teleseismic location techniques and their application to earthquake clusters in the south-central Pacific, *Bull. Seism, Soc. Am.* **71**, 1105-1130.

Kanasewich, E. R. (1981). *Time Sequence Analysis in Geophysics,* University of Alberta Press, Edmonton, Canada, 480 pp.

Langston, C. A. (1982). Aspects of *Pn* and *Pg* propagation at regional distances, *Bull. Seism. Soc. Am.* **72**, 1919-1929.

Leith, W. (1987). *Geology of NRDC seismic station sites in eastern Kazakhstan, USSR, U. S. Geol. Surv. Open-File Rept. 87-597.*

Mallick, S. and L. N. Frazer (1987). Practical aspects of reflectivity modeling, *Geophysics* **52**, 1355-1364.

Priestley, K. F., G. Zandt, and G. E. Randall (1988). Crustal structure in eastern Kazakh. USSR, from teleseismic receiver functions, *Geophys. Res. Lett.* **15**, 613-616.

Ryaboy, V. Z. (1989). *Upper Mantle Structure Studies by Explosion Seismology in the USSR,* DELPHIC Associates, Arlington, VA, 154 pp.

Thurber, C., H. Given, and J. Berger (1989). Regional seismic event location with a sparse network: application to eastern Kazakhstan, U.S.S.R., *J. Geophys. Res.* **12**, 17767-17780.

Vogfjord, K. S. and C. A. Langston (1991). Analysis of regional events recorded at NORESS, *Bull. Seism. Soc. Am.* **81**, 2016-2031.

DEPARTMENT OF GEOLOGY AND GEOPHYSICS
UNIVERSITY OF WISCONSIN-MADISON
1215 W. DAYTON STREET
MADISON, WISCONSIN 53706

2.4.2. Modified generalized ray modeling of regional seismograms in Central Asia

Introduction

The demise of the Soviet Union coupled with increased concerns of nuclear weapons proliferation monitoring is resulting in more research effort in the area of seismic wave propagation at regional distances (500 to 2000 km). This distance range is difficult to model accurately because it is too short to permit a teleseismic-like approach in which only the receiver-site influence on the waveform is of concern, and it is too long for a single source-region velocity model to be valid. Thus, waveform modeling methods that incorporate lateral heterogeneity are required.

A few researchers have attempted to model waveforms and crustal structure in the C.I.S. and Kazakhstan regions using single structure reflectivity or generalized ray models, with varying levels of success. Goldstein et al. (1992) modeled a number of nuclear explosions at station ARU using a reflectivity code. Their research gave a model of the mantle between 50 and 400 km depth in the region between the Kazakhstan test site and station ARU. This model showed a low velocity zone in the depth range between 150 and 200 km. Burdick et al. (1992) modeled data recorded at about 10 stations in Kazakhstan and the C.I.S. at distances between 1500 and about 5000 km for events recorded in the years between 1971 and 1989, using pre-existing velocity structures and the generalized ray method. They made no attempt to develop new, improved models. Both of these studies share two similar problems; first they require a common model at both the source and receiver, which does not allow for the effect of lateral heterogeneity in this region, and second an inability to model a large amount of the observed complexity of the data, especially the secondary arrivals in the time frame of 5 to 20 seconds behind the first arrival.

In a study of the receiver structure under the sites ARU, GAR, KIV, and OBN, Riviere-Barbier et al. (1992) used teleseismic P waveforms to model the velocity structure under these stations. They produced models which match the teleseismic data fairly well, deriving significantly different receiver structures for each station. However, their results do not match those of Burdick et al. (1992) or Goldstein et al. (1992). At station WMQ, M- agino and Ebel (1992) modeled teleseismic data to obtain a preliminary receiver crustal structure; however, they do not resolve the details of the upper mantle structure below 90 km depth.

In this section, we present crustal and upper mantle models under the stations BRV, FRU, NVS, and WMQ (Figure 1) which for FRU and NVS are the first known models at this site, and which for BRV and WMQ are the first models of the upper mantle. They are obtained from a modified generalized ray synthetic seismogram computation using a split source-receiver model which computes approximate synthetic seismograms for the first 10 or 20 seconds. Our results give a better fit to the data by nearly a second in first and second arrival times over results obtained

22

using a common source-receiver model. The source region structure in the depth range between 0 and 90 km is the Kazakhstan model obtained from reflectivity synthetic seismograms of chemical explosions determined by Quin and Thurber (1992). The mantle structure in the depth range from 90 to 200 km was obtained by matching the regional synthetics in the distance range of 600 to 1000 km. The upper mantle models show evidence for a moderate amount of lateral heterogeneity in this region; most, however, show an increase from 8.25 km/sec at about 50 km depth through 8.37 km/sec at 70 km depth to about 8.55 km/sec at 100 km depth.

Generalized Ray Model

The modeling procedure used in this section uses the generalized ray method of Helmberger (1972) but with a significant modification. The original generalized ray method assumes that the source and receiver have the same velocity model. However, regional refraction data indicates that the C.I.S. and Kazakhstan region exhibit considerable crust and mantle lateral heterogeneity (Ryaboy, 1989). An examination of the Cagniard integration method indicates that the amplitude and phase of the arriving waves can be broken down into separate functions of the source and receiver models, with the down-going wave propagating through the source region and the up-going wave propagating through the receiver region for the phases Pn, PmP and reflected waves which propagate through the mantle (Figure 2). The Laplace transform, s, of the generalized ray response is given by (Aki and Richards, 1980)

$$(1) \qquad P(r,z,s) = 2s/\pi R_s P_0(s) \text{Im} \int_0^{i\infty} K_0(spr)[PR(p)]exp(-s[SUM(p)])dp$$

where

$$(2) \qquad PR(p) = (PP)_{1s}(PP)_{2s} \cdots (PP)_{(n-1)s} (PP)_{ns}(PP)_{(n-1)r} \cdots (PP)_{2r}(PP)_{1r}$$

where PP_{ns} and PP_{nr} indicate the reflection and refraction coefficients of down-going (source) and up-going (receiver) waves, respectively, and where

$$(3) \qquad SUM(p) = (Th_{1s} - d_s)\xi_{1s} + Th_{2s}\,\xi_{2s} \cdots + Th_{(n-1)s}\,\xi_{(n-1)s} + Th_{ns}\,\xi_{ns} + Th_{(n-1)r}\,\xi_{(n-1)r}$$
$$\cdots Th_{2r}\,\xi_{2r} + (Th_{1r} - d_r)\xi_{1r}$$

where Th_i is the thickness of each layer and d_s and d_r are the source and receiver depths, $\xi_i = (\alpha_i^2 - p^2)^{1/2}$ is the ray parameter weighting factor for each layer, R_0 is the distance from the source to the receiver, $P_0(s)$ is the Laplace transform of the initial pressure pulse, and $K_0(spr)$ is a

23

modified Bessel function. The Cagniard path for inversion of equation 1 is now the solution of $p = p(\tau)$ where $\tau = pr + \text{sum}(p)$.

The split source receiver method entails solving for the functions PR(p) and SUM(p). These equations can be split into two parts: a downward part $PP_{1s}PP_{2s}PP_{3s}$... and an upward part $....PP_{3r}\,PP_{2r}\,PP_{1r}$ (note that for the case of converted waves we would replace the terms PP by PS, SS or SP). For SUM(p) we need to solve the equation $p = p(\tau)$ for τ numerically in order to find the Cagniard integration path for each ray. This solution begins with an initial ray parameter on the real axis obtained from the P wave slowness of the deepest layer in which that ray penetrates. Subsequent values of the complex ray parameter p for each time point on the seismogram are obtained from an iterative method in which the initial guess of the complex ray parameter arriving at that time step is obtained from the last ray parameter and the direction of the ray parameter contour at the last time step.

In terms of modification of the generalized ray program, the subroutine which determines the Cagniard travel time is modified to incorporate the split source receiver structure, with a slight change in the ray parameter computation routine to account for rays which do not converge. In practice the solution to this equation can be found for about 99% of all possible rays arriving in the first 20 seconds after the first P wave, including all of the most important rays; the only rays for which a ray parameter path cannot be found are for a few late arriving highly converted phases. Therefore, we believe our method is an effective approximation procedure for the split source-receiver case.

Our model treats the source-receiver boundary as being exactly at the mid-point of the source-receiver distance. In reality, this boundary could be located anywhere; and, in theory, the wave integral could be split up so that multiply reflected phases could be treated as if they propagated through more than two distinct regions with different phase factors and different refraction coefficients for each set of layers, as long as a solution for the ray parameter equation can be found. However, we know from the work of Quin and Thurber (1992; section 2.4.1) that the Kazakhstan region does not show significant heterogeneity in the distance range less than about 300 km from the source, and that most lateral heterogeneity occurs in the crustal region, where the model of waves traveling downwards from the source and upwards to the receiver is most appropriate. Also, the upper mantle in this region shows only limited heterogeneity; computing the mantle velocity for head waves using the average mantle velocity gives an incorrect velocity by at most 0.03 km/sec, well within the accuracy of the known arrival times. In addition, surface reflection phases 2PmP and 2Pn can be considered to propagate through a source region, bounce off the free surface, and propagate through a receiver region of different crust and upper mantle structure. Therefore, we can use the same split source-receiver approximation for these phases as

24

well. This means that we can model almost all phases arriving in the first 20 seconds in the distance ranges of interest for these seismograms using the split source-receiver model.

The synthetic seismograms are sampled at 20 Hz and inverse Fourier transformed at a sampling length of 1024 points, and then low pass filtered with a corner frequency of 2 Hz. This enables us to get a good sampling of the important phases, and to filter out high frequency noise. We incorporate attenuation using the standard constant Q attenuation model with a Q value of 500, a value typical of crustal P waves in this region (Sereno, 1990). This gives us a reasonable value for attenuation in this region, eliminating unphysical high frequency arrivals. Using this method we can reproduce most of the important first arriving phases seen in the time frame of the first 20 seconds of data.

To test the accuracy of the program we compared synthetic seismograms from a single model with those computed by the separate source-receiver model method for the case of identical crustal structures and find that the two methods give identical results. For the case where the two models are different we have found that the split model enables us to produce a much better fit to the arrival times and phases than the single structure model (Figure 3). This figure shows both BRV and WMQ waveforms computed at a distance of 670 and 800 km. Our split model gives a better fit to the data than the single model. In particular, we are able to accurately match both the first and second arrival times and the overall waveform envelopes better with our approach. We believe our approach more effectively incorporates the known crustal and upper mantle lateral complexity as determined by refraction and teleseismic data than efforts based on single structure models.

Regional Data

Data from a number of different sources were utilized in this study. Tables 1 and 2 summarize the stations and event data used in this study. The quality and type of data used varied from station to station. For stations FRU and NVS the data consist of intermediate period vertical hand-digitized data from explosions in the Kazakhstan and Konystan regions in 1965-1989; at stations BRV and WMQ the data consist of high quality broad band 3-component recordings made in 1988. All of the data at stations WMQ and BRV are usable; however, a large number of the waveforms at stations FRU and NVS are incomplete or inaccurate.

We have taken the usable waveforms from sets of events with epicenters within about 3 km of each other as determined from satellite images and teleseismic relocations (Lilwall and Farthing, 1990, Thurber et al., 1992), deconvolved the station responses and stacked them to obtain 3 or 4 different modelable waveforms at each station. A large number of these waveforms are clipped and inaccurately timed; however, about a dozen or so were usable. These waveforms span four distances in the range 621-676 km at stations NVS and 813-847 km at station FRU. At stations

BRV and WMQ, we low pass filtered with a corner frequency of 2 Hz and rotated the broadband data from several nuclear explosions recorded in the years 1972-1989 to get good quality waveforms in the distances between 683-697 km at BRV and 950-962 km at WMQ. After comparing both stacked and unstacked data at BRV and WMQ against the synthetics, we decided to model the unstacked data, due to the high quality of the data and the high accuracy with which the explosion locations after 1986 were known from satellite and teleseismic data (Thurber et al., 1992; section 2.4.3).

Explosion Source Model

The manner in which the characteristics of the nuclear explosion source are quantified has been studied in considerable detail in both the near and far field. In general, the details of the manner in which the source is described depends greatly upon the distance range at which it is observed; in the far field, the explosion source appears simply an as isotropic point force right below the surface, while in the near field the source appears as a complex nonlinear shock wave. Day (1983) and Von Seggern (1988) have studied the effect of source depth and spallation between 100 and 1000 km from the explosion source. In particular, they have concluded that both source depth and spallation are important in the generation of the regional phase Lg, especially since this phase cannot be successfully modeled using simple planar models and linear point explosion terms.

Their computation of the phases Pn and pPn, the near surface reflected phase, indicate that to first order the near surface velocity and the source depth are the most important parameters controlling the generation of these phases in the mid-regional case. Nonlinear effects appear as second order effects which cannot be distinguished in the data from models in which the timing and amplitude of these phases are modeled using an elastodynamic representation theorem. In addition, our generalized ray method does not allow for nonlinear source effects to be incorporated in our models. Therefore in this report we have ignored nonlinear near source effects and simply approximated the explosions as point sources with an isotropic moment tensor at an average depth of 0.5 km, a depth chosen as the average obtained from empirical magnitude estimates of depth (Jih and Wagner, 1991), and included the surface reflection phases pPg, and pPn. For the explosion source time function we use the standard explosion model of Mueller and Murphy (1971) which consists of a sinusoid multiplied by an exponential term, which simulates the effect of a sharp outward pulse, followed by an inward elastic rebound.

Modeling Procedure

The modeling procedure consisted of a two stage process. In stage 1, we modeled the arrival time and phase of the first arrivals using the phase Pn, which a travel time analysis indicates

26

was the first arriving phase in the region between 600 and 1000 km. We have an adequate model of the crust and upper mantle structure in the Kazakhstan source region from the earlier modeling work of Quin and Thurber (1992). Our Kazakhstan crust and upper mantle structure (Figure 5) has a low velocity crust of 5.0 km/sec in the upper 10 km, a middle crustal layer of about 6.95 km/sec and an upper mantle velocity of 8.25 km/sec. Between 70 and 95 km depth the source models have a velocity of 8.35 km. We have adopted this crust and upper mantle model as the source model for our study; all of the rays propagate downward through this crust and upper mantle model in the region between 0 and 70 km depth. With the source structure fixed, we use the Pn arrival times and, starting with crustal models based on earlier work, determine the best fitting receiver crust and uppermost mantle structures in each region. This fixes the receiver model down to about 50 km.

With the crustal structure determined, we determine the upper mantle structure by modeling the distinct secondary phases observed in the data arriving up to 10 seconds after the Pn phase. Our investigation indicates that these second arrivals are generally influenced by the structure in the upper mantle; in particular, the arrivals in the first 5 seconds after the Pn arrival are affected by structure in the 50 to 90 km depth range, while arrivals in the 5-15 sec time span are affected by the 90 to 200 km depth range. We believe our models resolve details of the crust and upper mantle structure in this region down to a depth of about 200 km for events in the distance range up to 1000 km from the source.

We allowed the source mantle velocity in the region between 70 and 150 km depth to be a variable in our study. This at first may appear inconsistent; however an examination of the path of the waves indicates that they are separated at this depth by as much as 500-600 km, which means that the waves propagate through different tectonic regions towards each station. We allow the velocity structure to vary by about 0.25 km/sec between the various models in this region, consistent with the observed lateral heterogeneity in this region (Riviere-Barbier et al., 1992); the source model at station BRV shows a velocity of 8.25 km./sec in the region between 70 and 90 km, and a low velocity zone in the region between 110 and 130 km while the other models didn't.

For waves propagating to stations NVS and WMQ the best fitting source model had a velocity of 8.35 km./sec at 70 and 90 km depth, and a velocity of 8.50 km/sec in the region between 90 and 110 km depth. At station FRU, we find that the best fitting source model had a high velocity region of 8.50 km/sec in the region between 90 and 130 km depth. In the region between 110 and 130 km, NVS and FRU have a velocity of about 8.55 km/sec, while all the models have a velocity of 8.60 km/sec below 130 km depth down to 200 km depth. This variation of the source crustal and upper mantle model at depth allowed us to get a better fit to the synthetic seismograms.

27

About a dozen trial and error modeling attempts were required at stations FRU and NVS, for which we did not have good starting models. At stations WMQ and BRV, for which we have useful starting models obtained from teleseismic data, only about four or five trials were needed. The fit of the synthetics to the data varies from station to station (Figure 4). At station NVS, we match the first arrivals and the timing of the second and third arrivals fairly well; however, we have difficulty in matching the amplitude of the second arrival about 2 seconds after the first arrival. At station FRU, the first arrival of the synthetic is about a half second early, and we find that the third synthetic arrival about 6 seconds after the first P wave come in too strongly, regardless of what mantle model we utilize. We do match the timing and amplitude of the second arrivals in the period about 2-3 seconds after the first arrival.

At stations BRV and WMQ, we are able to model both the vertical and rotated radial waveforms. At station BRV, we are able to match both the first arrival time of the phase Pn and the overall waveform envelope in the following 10 seconds; however, our model somewhat overestimates the first arrival amplitude compared to the coda. At station WMQ, we match the first arrivals and the overall waveform envelope. We do not get a good match to the second arrivals in the next few seconds after the first arrival on the vertical component, although on the radial component we match the arrival times of both first, second and third arrivals. Overall, given the simplicity of our models, the complexity of the crustal structure in this region and the high frequency character of the data, the fit is better than expected. Our split models give a much better fit than the single crustal structure model, as shown in Figure 3.

Discussion of Receiver Models

An examination of regional refraction data and teleseismic arrival time data (Ryaboy, Suteau-Henson 1989) indicates that considerable lateral heterogeneity exists in both the crust and upper mantle structure in this region, corresponding to the differing tectonic provinces in which the waves travel; in the region north of the test site, the waves travel through a shield region; to the west they travel through the Caucasus region, while to the south and east they travel through the thick crustal region of the Tien Shan. This lateral heterogeneity shows up in the various crustal and upper mantle models for the receiver structures.

These differing crustal and upper mantle structures give significantly different arrival times for the various regions. This heterogeneity is incorporated in our starting models. For the stations NVS and FRU, for which no previous source structure model exists, we use the average of the source model and the nearest known receiver structure as the starting model. For the starting model for station BRV, we use the crust and upper mantle structure of Oreshin, et al. (1992) as obtained by teleseismic modeling of P wave data. At station WMQ, we utilize the starting model of Mangino and Ebel (1992) to obtain a starting receiver crustal structure. We then systematically

28

vary these models to get the best fitting velocity model in each region. Our receiver models have a fair amount of nonuniqueness; it is difficult to determine exact receiver structures solely on the basis of our work. Our models represent the best fit of modified preexisting receiver models to the data at BRV and WMQ, and the best fit of regional known crustal and upper mantle structures to the data at NVS and FRU. We have much more confidence in the accuracy of our BRV and WMQ models, for which we have both quality data and accurate starting models, than at NVS and FRU, for which we do not.

Our final models show considerable similarity; however, the location of the crust mantle boundary varies from location to location, as does the upper mantle transition depth from 8.30 km/sec to 8.55 km/sec. At station NVS, the crust has a thickness of 50 km depth with a lower crustal layer of 7.20 km/sec lower crustal layer between 30 and 50 km depth. The upper mantle velocity in the region between 50 and 70 km has a velocity of 8.23 km/sec, a velocity of 8.35 km/sec in the region between 70 and 90 km depth, and a velocity of 8.50 km/sec in the region between 90 and 110 km depth.

At station FRU, the Pn first arrival indicates a high velocity upper crustal layer of about 6.0 km/sec in the upper 10 km with a 6.5 km/sec lower crustal layer of 20 km thickness between 10 and 30 km depth and a lower crustal velocity of 7.0 km/sec in the region between 30 and 45 km.depth. The upper mantle in the region between 45 and 65 km depth has a velocity of 8.25 km/sec, a velocity of 8.35 km/sec in the region between 70 and 90 km depth, a velocity of 8.55 km/sec in the region between 90 and 110 km depth, and a velocity of 8.65 km/sec in the region between 110 and 250 km depth.

At station BRV, our model is similar to that of Oreshin et al. (1992). We find that the crust has a thickness of about 50 km with a mid-crustal velocity of 6.5 km/sec and a lower crustal velocity of 6.8 km/sec, with a sharp transition at 50 km depth to an upper mantle velocity of 8.25 km/sec extending down to about 90 km. In the region between 90 and 110 km depth, the mantle has a velocity of 8.37 km/sec, and a velocity of 8.25 km/sec between 110 and 130 km depth. Below 130 km depth the mantle has a velocity of 8.60 km/sec.

At station WMQ, our model is similar to that of Mangino and Ebel. The crustal depth under station WMQ is 55 km, with a low velocity crustal gradient in the upper 10 km, a mid crustal velocity of 6.5 km/sec in the region between 10 and 30 km depth, and a lower crustal velocity of 7.0 km/sec. The upper mantle has a velocity of 8.25 km/sec down to 75 km depth, a lower upper mantle velocity of 8.37 km/sec down to 95 km, a low velocity zone of 8.25 km/sec between 95 and 120 km depth, a velocity of 8.55 km/sec down to 180 km, and a velocity of 8.70 km/sec below 180 km depth. The low velocity zone was needed in order to match the observed arrival times in the late phases of the data.

In comparison to earlier work, we find that most of our crustal structures show the greatest resemblance to the U.S.S.R. shield models of Riviere-Barbier et al. (1992), which show a crust mantle boundary at about 43 km depth in the shield regions in the C.I.S. and a transition from about 8.30 km/sec to about 8.55 km/sec at 90 km depth. Our models somewhat resemble the U.S.S.R. shield models of Burdick et al. (1991); however, as they are unable to exactly identify the correct model for each region, comparison with their work is difficult. Our BRV model better resolves the details of the upper mantle structures of Oreshin et al. (1992), and our WMQ model better resolves the details of the mantle than the structure of Mangino and Ebel (1992). All of our receiver structures incorporate a layered crustal model in the upper 10 km to account for the gradient in the velocity in the upper crust, as shown in previous source studies.

Source Depth from Regional Seismograms

One of the questions raised by our research is whether our split-source receiver model offers the possibility of determining the depth of an event, and whether our results are useful in solving the problem of earthquake-explosion discrimination. In order to test the utility of our split-source receiver model, we computed synthetic seismograms for 2 sets of models in a slightly simplified six layer crustal structure (Figure 6). We computed seismograms at a distance of 955 km for a receiver structure similar to that of WMQ and at a distance of 685 km for a receiver structure similar to that of BRV. We examine a range of explosion and earthquake source depths for each model. For the explosion source model we used source depths of 0.2, 0.4, and 0.8 km depth, typical of what would be expected at a drilled test site. For the earthquake source model, we used a source depth of 5 km typical of those found in the upper crust.

We computed Green's functions and convolved them with two different source time functions. For the explosion source, we used the standard Mueller-Murphy source as reported earlier. For the earthquake source model, we used a trapezoidal time function of about 1 second duration for a strike slip earthquake similar to that of a magnitude 5 earthquake. We low pass filtered the resulting events with a low pass filter with a cutoff of 2 Hz. We find that for the explosion model, there are slight changes in the character of the seismograms depending on source depth; the deeper explosion events have a slightly greater high frequency component directly after the first P wave arrival. The earthquake waveforms are not readily distinguished from the explosion waveforms. Thus we are uncertain whether our work can be used definitively for earthquake-explosion discrimination.

Conclusions

We computed generalized ray synthetic seismograms of explosions for events recorded in the C.I.S. between 1971-1989. Our split source-receiver model computes the Cagniard ray parameters using the split source-receiver phase arrival times, and the ray amplitudes using the multiplied reflection and refraction coefficients. We were able to produce seven and eight layer models which incorporate regional refraction data and which match both the timing and relative amplitudes of the first and second arrivals in the first 10 seconds of the data using our split model.

Our source model was obtained from the work of Quin and Thurber (1992). This model had a crust-mantle boundary at about 45 km depth, an upper mantle velocity of 8.25 km./sec between 45 and 70 km depth, a velocity of 8.37 km/sec in the region between 70 and 90 km, a low velocity zone of 8.25 km/sec in the region between 0 and 110 km depth and a velocity of 8.65 km below 130 km. Our receiver models show variety of crust and upper mantle structures. Stations NVS, BRV, and FRU have a crust-mantle boundary of about 47 km depth, while station WMQ has a crustal depth of 55 km. Most receiver models had an upper mantle velocity of 8.25 km/sec in the region between 50 and 70 km depth and a mid-upper mantle velocity of 8.65 km/sec in the region below about 130 km depth. Our modeling results may be useful in improving our ability to discriminate between earthquakes and explosions, and in determining the source depth of earthquakes.

31

Table 1. Summary of stations and stacked distance ranges for events at each station

Station	Latitude	Longitude
BRV	53.0548	70.2763
FRU	42.8333	74.6167
NVS	54.9000	83.3000
WMQ	43.8210	87.6950

Stations and epicentral distances (in km) for waveforms

BRV	FRU	NVS	WMQ
683	813	621	650
686	819	665	655
691	830	670	658
697	847	676	662

Table 2. Summary of event locations and dates used

Event Date	Latitude	Longitude	Depth (km)	Distance (km)	# waveforms
			FRU		
78085	49.730	78.070	0.4	811.7	1
78209	49.740	78.160	0.4	815.1	1
80143	49.720	78.160	0.5	811.5	1
84106	49.740	78.160	0.4	815.1	1
82050	49.800	78.110	0.5	820.1	2
87126	49.830	78.130	0.5	823.7	2
87198	49.800	78.110	0.5	820.1	2
71157	49.980	78.770	0.4	830.0	3
78162	49.989	78.785	0.5	848.7	4
78246	49.921	78.925	0.4	855.1	4
85241	49.947	78.786	0.5	853.6	4
			NVS		
79230	49.947	78.918	0.5	626.8	1
87057	49.840	78.120	0.4	664.7	2
87126	49.830	78.130	0.5	665.3	2
78209	49.740	78.160	0.5	672.9	3
78241	49.830	78.000	0.4	670.0	3
82050	49.800	78.110	0.5	668.9	3
84106	49.740	78.160	0.4	672.9	3
75159	49.760	78.080	0.5	673.8	4
78085	49.730	78.070	0.4	677.1	4
			BRV		
78241	49.830	78.000	0.5	685.0	1
72345	49.840	78.090	0.5	686.0	1
88094	49.921	78.909	0.5	693.6	2
88044	49.932	78.808	0.5	687.0	2
88317	50.047	78.969	0.4	689.5	2
80286	49.967	79.019	0.6	697.4	3
88166	50.036	79.967	0.4	696.1	3
			WMQ		
88094	49.921	78.909	0.5	952.0	1
88352	49.880	78.924	0.5	948.0	1
88316	49.878	78.824	0.5	953.0	2
88044	49.932	78.868	0.5	955.0	2
88258	50.036	78.969	0.5	958.2	3
88316	50.047	78.969	0.5	958.8	3
88166	49.945	78.754	0.4	962.0	4

33

Figure 1. Epicenter and station location map.

Figure 2. *Illustration of ray paths for a split source receiver model showing the paths Pn, PmP, Pg, 2PmP and 2Pn, and other crustal and upper mantle phases.*

Figure 3. Comparison of synthetic seismograms at stations NVS and WMQ computed using single model method and double model method compared with data. Traces are, in order, split model, source only model, receiver only model, and data.

Figure 4. Data recorded at stations FRU, NVS, BRV, and WMQ (bottom in each panel) compared with synthetic seismograms (top in each panel).

Figure 5. Velocity models showing source model and receiver models for each station.

Figure 6. Synthetic seismograms for explosions computed at depths of 0.2, 0.4 and 0.8 km depth compared against a strike slip earthquake computed at a depths of 5 km (a) at a distance of 955 km for a receiver structure similar to that of WMQ and (b) at a distance of 685 km for a receiver structure similar to that of BRV.
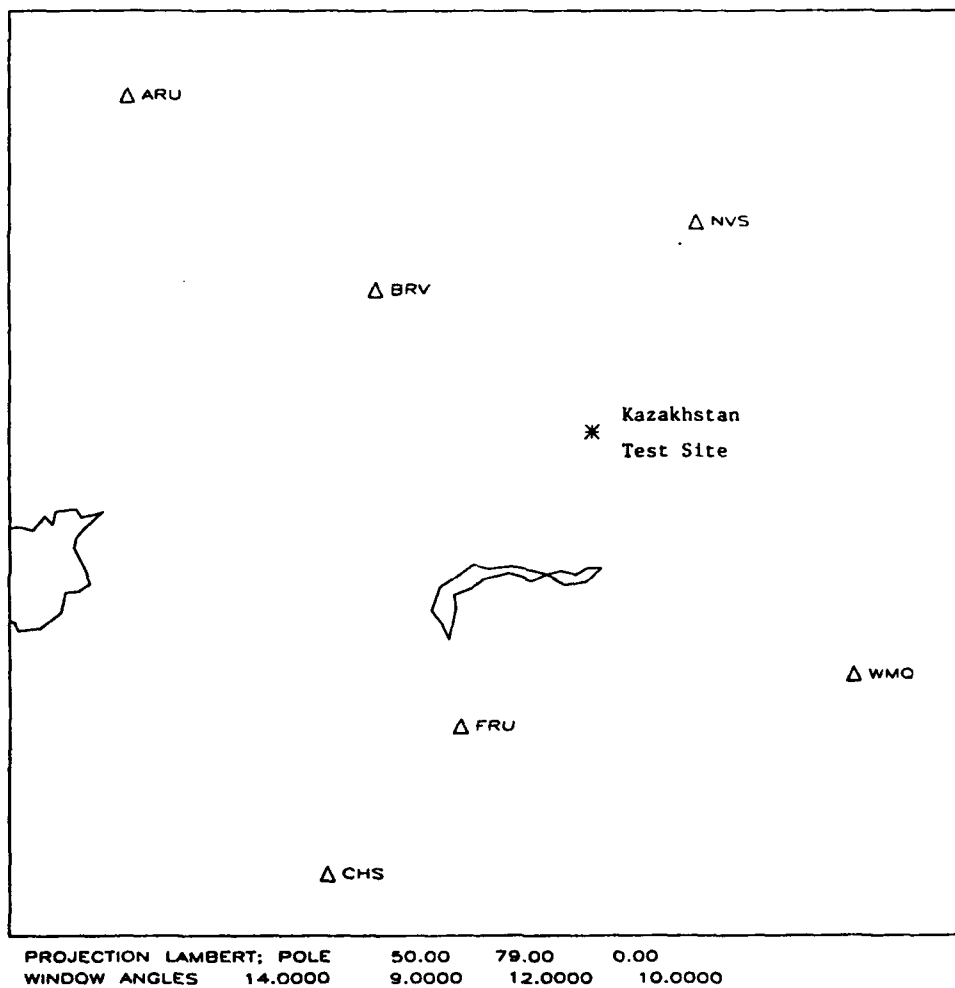
PROJECTION LAMBERT; POLE   50.00   79.00   0.00
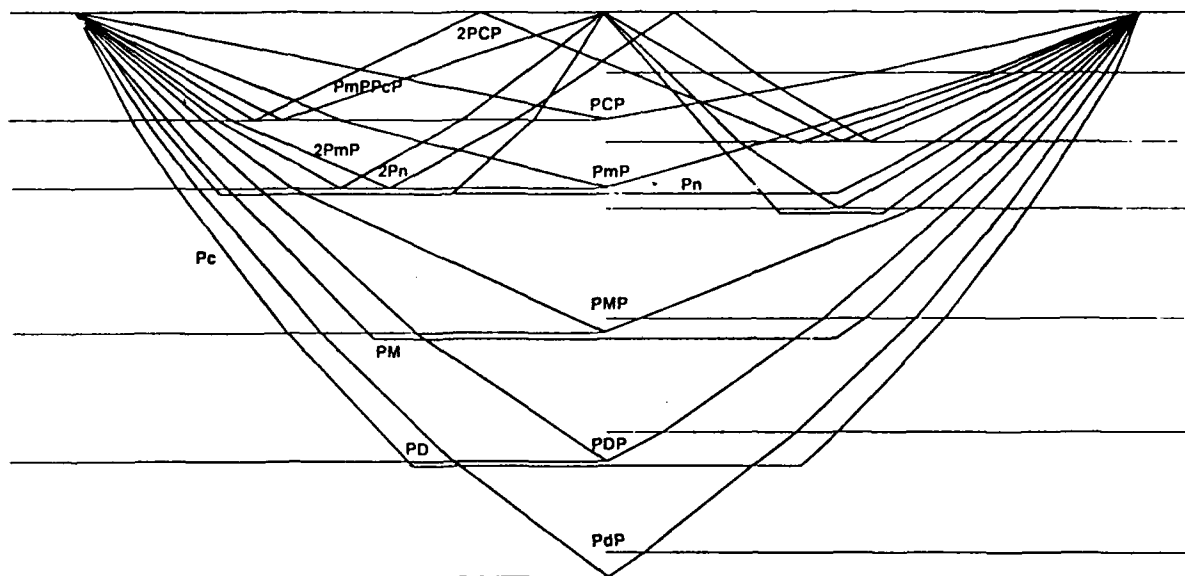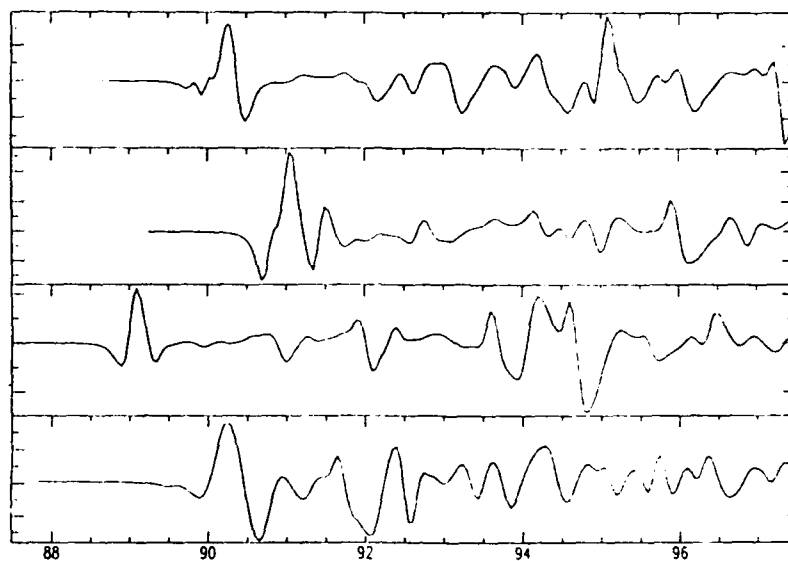WINDOW ANGLES   14.0000   9.0000   12.0000   10.0000

Figure 1

Figure 2

36

NVS 670.0

WMQ 960.0

Figure 3

BRV 687.0

FRU 846.0

WMQ 960.0

NVS 670.0
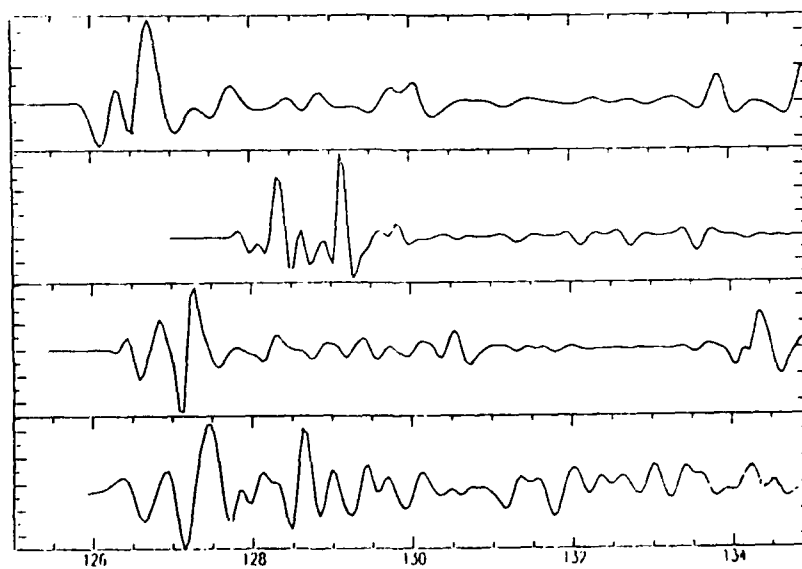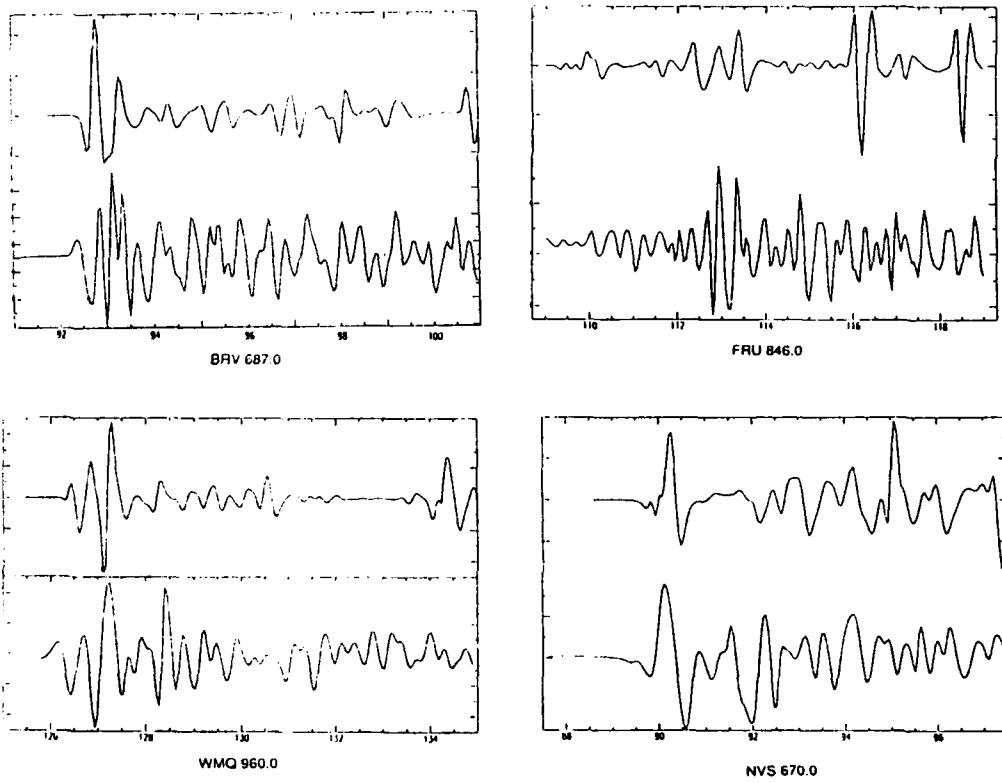
Figure 4

Figure 5

(a)

BRV 685

(b)

WMQ 955
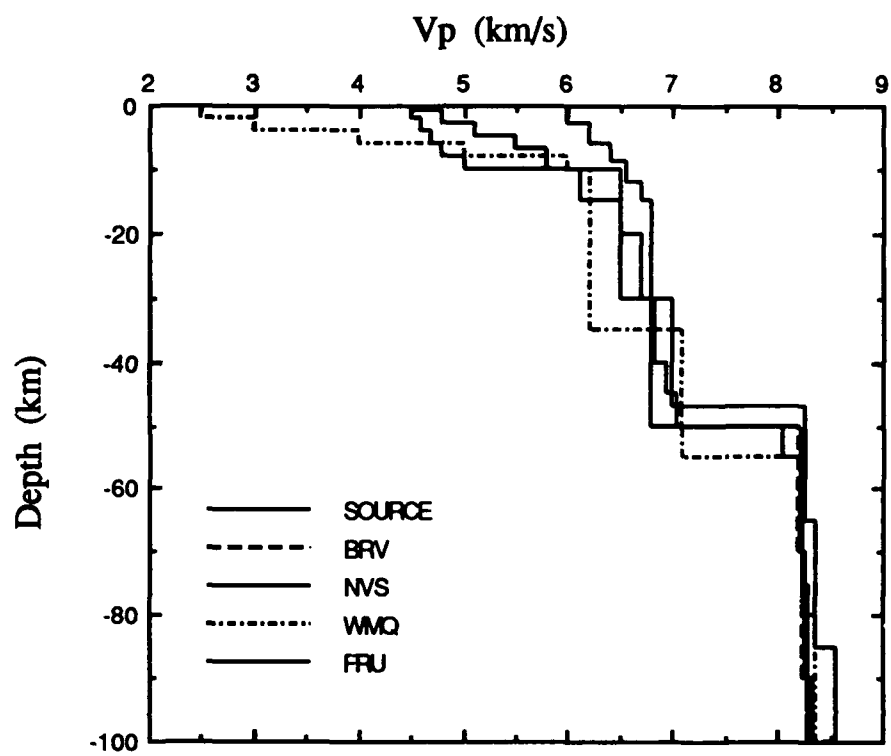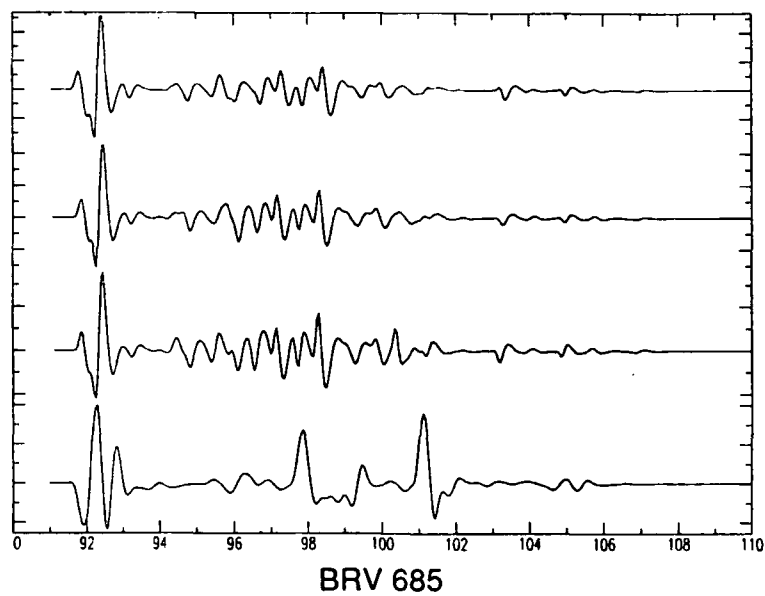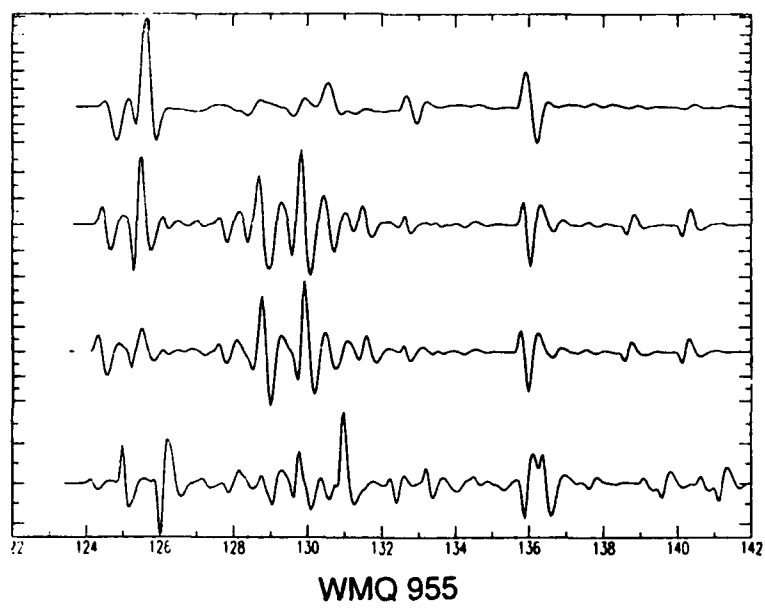
Figure 6

40

2.4.3. Accurate locations of nuclear explosions at Balapan, Kazakhstan, 1987 to 1989

C. H. Thurber and H. R. Quin

Department of Geology and Geophysics, University of Wisconsin-Madison

P. G. Richards

Lamont-Doherty Earth Observatory of Columbia University

Abstract. Locations of 20 nuclear explosions from 1987 to 1989 at the Balapan test site, Kazakhstan, are derived with a precision of about 100 m from time-sequence SPOT satellite images combined with teleseismic epicenter estimates. For most events, there is little or no ambiguity in the association between seismic events and image features. The locations determined by JED are associated with formal error estimates (95% confidence ellipses) that are significantly too small. In 16 out of 19 cases, the events are found from satellite imagery to lie outside these ellipses. Possible causes are nonuniform observation, poor azimuthal coverage, and source region heterogeneity. Our results should prove valuable for studies of seismic waveforms, arrival time and amplitude tomography, event location, tectonic release, and seismic coupling at Balapan, and demonstrate the utility of combined seismic and satellite image analyses for seismic verification studies.

Introduction

The former Soviet Union conducted its last nuclear explosion at the Kazakhstan (Semipalatinsk) Test Site (KTS), in East Kazakhstan, in October, 1989. In August 1991, the newly independent country of Kazakhstan closed the test site and in May 1992 undertook to enter the Non-Proliferation Treaty as a non-nuclear weapon state. Prior to its closing, several hundred nuclear explosions had been conducted underground in Kazakhstan, making KTS second in numbers of explosions only to the Nevada Test Site of the U.S.

The signals of nuclear explosions are of great interest since they permit detailed studies of earth structure and properties in the source region. To address these issues, it is often necessary to obtain very accurate locations for the explosions. Perhaps the greatest potential is in "source array" studies (e.g., Goldstein et al., 1992; McLaughlin et al., 1992), wherein a precise knowledge of source locations allows a controlled study of propagation effects. The study of tectonic release could be advanced greatly by having accurate locations of explosions with respect to nearby faults. Many other travel time, amplitude, waveform, and source location issues can also be executed at levels of precision not possible with earthquake sources, once accurate explosion locations are available. In this paper, we give estimates, to a new level of precision, of the locations of 20 nuclear explosions in the Balapan area of KTS between 1987 and 1989.

Information on the locations and characteristics of 96 KTS explosions prior to 1973 has been made publicly available by Bocharov et al. (1989) and reported in the U.S. literature by Vergino (1989a,b). Of these events, 7 were from Balapan (Shagan River) subregion of KTS. There have been a number of teleseismic joint location studies, such as Marshall et al. (1984) and Lilwall and Farthing (1990). The Marshall et al. (1984) study used the location of the January 1965 cratering explosion in a LANDSAT image to provide a master event for their analysis. Lilwall and Farthing (1990) included nearly all of the events listed by Bocharov et al. (1989) as master events.

We report the results of a simple and direct approach to the determination of accurate locations for recent (post 1986) KTS explosions in Balapan by combining time-sequence satellite images of KTS with the known location information and teleseismic location estimates. High-resolution images of Balapan from Satellite Pour l'Observation de la Terre (SPOT) are available at irregular intervals between 1986 and late 1989: 860617, 870807 (partial coverage), 880826, 881011, 890603, 890708 (partial coverage), and 89101. Fresh features can be associated with explosions occurring in the corresponding time period. We estimate our final location errors to be about 100 m, based on comparisons between our locations and (a) those available for a small number of events, and (b) those picked independently by one of us from two SPOT images available at the DARPA Center for Seismic Studies in Arlington, VA.
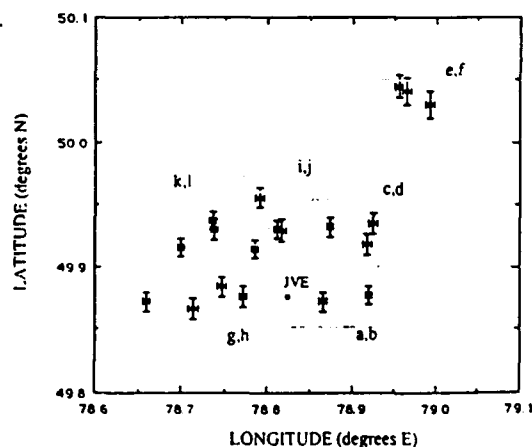

Fig. 1. JED locations of the most recent 20 Balapan nuclear explosions (post 1986) with the 1988 JVE used as the master event. The dashed boxes indicate the areas of the SPOT images shown in Fig. 2.

Table 1. JED locations for Balapan explosions, 1987 - 1989

N	YrMoDa	Lat (°N)	±km	Lon (°E)	±km	Depth (km)	m_b[†]
82	870312	49.9309	1.0	78.8166	0.6	0.3	5.3
83	870403	49.9156	0.8	78.7844	0.4	0.5	6.1
84	870417	49.8738	0.9	78.6585	0.4	0.5	5.9
85	870620	49.9319	0.9	78.7372	0.4	0.5	6.0
86	870802	49.8739	0.9	78.8649	0.5	0.4	5.8
87	871115	49.8856	0.9	78.7452	0.5	0.5	6.0
88	871213	49.9577	0.9	78.7897	0.5	0.5	6.1
89	871227	49.8681	0.9	78.7135	0.5	0.5	6.0
90	880213	49.9340	0.9	78.8737	0.4	0.5	6.0
91	880403	49.9198	0.9	78.9185	0.4	0.5	6.0
92	880504	49.9388	0.8	78.7352	0.4	0.5	6.1
93	880614	50.0430	1.2	78.9651	0.6	0.2	4.8
94*	880914	49.8781	0.0	78.8239	0.0	0.5	6.0
95	881112	50.0473	1.0	78.9558	0.5	0.3	5.2
96	881217	49.8791	0.8	78.9191	0.4	0.4	5.8
97	890122	49.9318	0.8	78.8107	0.4	0.5	6.1
98	890212	49.9180	0.8	78.6983	0.4	0.5	5.9
99	890708	49.8776	0.9	78.7713	0.4	0.4	5.6
100	890902	50.0316	1.2	78.9929	0.6	0.2	4.9
101	891019	49.9370	0.9	78.9258	0.4	0.5	5.9

*JVE

[†]from Ringdal et al. (1992)

JED Analyses of Balapan Explosions

The studies of Marshall et al. (1984) and Lilwall and Farthing (1990) both utilized the JED method of Douglas (1967) to determine locations of KTS explosions using one or more master events. The Marshall et al. (1984) study included 61 explosions at Balapan through 1982, and used just the 1965 cratering event (event 650115) as a master event. The Lilwall and Farthing (1990) study included an additional 40 Balapan events from 1983 through the cessation of testing in 1989, and used all 7 Balapan events listed by Bocharov et al. (1989) as master events. The consistency between the locations of the 61 common events in the two studies is quite good, with an RMS difference of only about 1 km. Or own analysis using both JED and algorithm MLOC (E. Bergman, *personal comm.*, 1992) indicate the locations are stable within about 1 km. The main point of this paper is that with satellite images we can improve this precision by about a factor of 10.

Preliminary locations of the 20 post-1986 explosions at Balapan and their estimated uncertainties are shown in Figure 1 and Table 1, computed using algorithm JED (Douglas, 1967) and ISC data, with the epicenter of the JVE fixed at its image location. Event depths were fixed by scaling to magnitude with the formula of Jih and Wagner (1991), $\log(DOB) = 0.31\ m_b + 0.835$ (Table 1). These locations provide the starting point for analysis of the SPOT images.

Satellite Image Analysis

Nine events from the Bocharov et al. (1989) list were employed as control points for image rectification, 7 from Balapan and 2 nearby throwout craters known as T-1 and T-2 (Leith and Simpson, 1990). However, we suspect that the location of event 7 is in error in Bocharov et al. (1989), as there is a cratered feature at that location (possibly event 10, m_b = 4.4, 740416). Murphy and Jenab (1992) associate event

7 with the same faint feature chosen by us (at 50.0356, 79.0108), about 1.5 km northeast of the location provided by Bocharov et al. (1989). The rectification produced an excellent fit to the control points (RMS misfit of about 50 m).

Identifying the sites of the post-1986 explosions involved the comparison of the time-sequence SPOT images with the estimated event locations indicated in Table 1. Figure 2 shows "before-and-after" images acquired on 860617 and 891015 of areas containing identified explosion sites. The images are 8 km by 6 km, and their locations are indicated in Figure 1. The coordinates and event associations are presented in Table 2.

Figures 2a and b show the 1988 JVE (event 94, 880914) and the adjacent events 86 (870802) and 96 (881217). SPOT images exist both before and after each of these events, so these associations are quite certain. Coordinates for the JVE have been published by Murphy and Jenab (1992); their location of 49.8788° N, 78.8225° E agrees well with our estimate of 49.8781° N, 78.8239° E (less than 130 m apart). Figures 2 c and d cover the area just north of the JVE, with events 90 (880213), 91 (880403), and 101 (891019). Event 101 post-dates the last SPOT image, but the preparation area for the explosion (on October 19) is visible in the image of 891015. Because events 90 and 91 are well-separated both from each other and from other events close in time, it is unlikely that their identities are in error. Figures 2 e and f cover far NE Balapan with events 93 (880614), 95 (881112), and 100 (890902). There is complete before-and-after coverage for these events. The difficulty of distinguishing the emplacement point for 100 from a probable nearby trailer area lend some uncertainty to this association. Figures 2 g and h cover the area just west of the JVE with events 84 (870417), 87 (871115), 89 (871227), and 99 (890708). The lack of coverage of the western area in the 800807 image hinders our association effort. The feature identified as shot 84 is present in the 860617 image, though its appearance has changed in the next available image (880826). Events 87 and 89 are far enough apart from each other and other nearby events that their identification is reasonably certain despite their closeness in time. For event 99, we have excellent before-and-after coverage, so its identification is quite certain. Our location for this event of 49.8675 N, 78.7792 E is only about 70 m different from the location of 49.8681 N, 78.7792 E provided to us by Adushkin et al. (1992) after we had prepared our Table 2. Figures 2 i and j cover the area just north of the JVE with events 82 (870312)), 88 (871213), and 97 (890122). Again, because event 82 is spatially well-separated from other events close in time, it is unlikely that its identity is in error. We have complete before-and-after coverage for events 88 and 97, so these associations are quite certain. Figures 2 k and l cover the area NW of the JVE with events 83 (870403), 85 (870620), 92 (880504), and 98 (890212). Our associations for events 83 and 98 have high confidence; note also the apparent observation point to the ENE of event 98. For event 85, it is possible that the shot point is actually the smaller feature ESE of our pick; we interpret that to be an observation point. Our association for event 92 is somewhat less certain, but there is a relatively fresh feature visible in multi-spectral images that is not readily apparent in panchromatic images.

Discussion and Conclusions

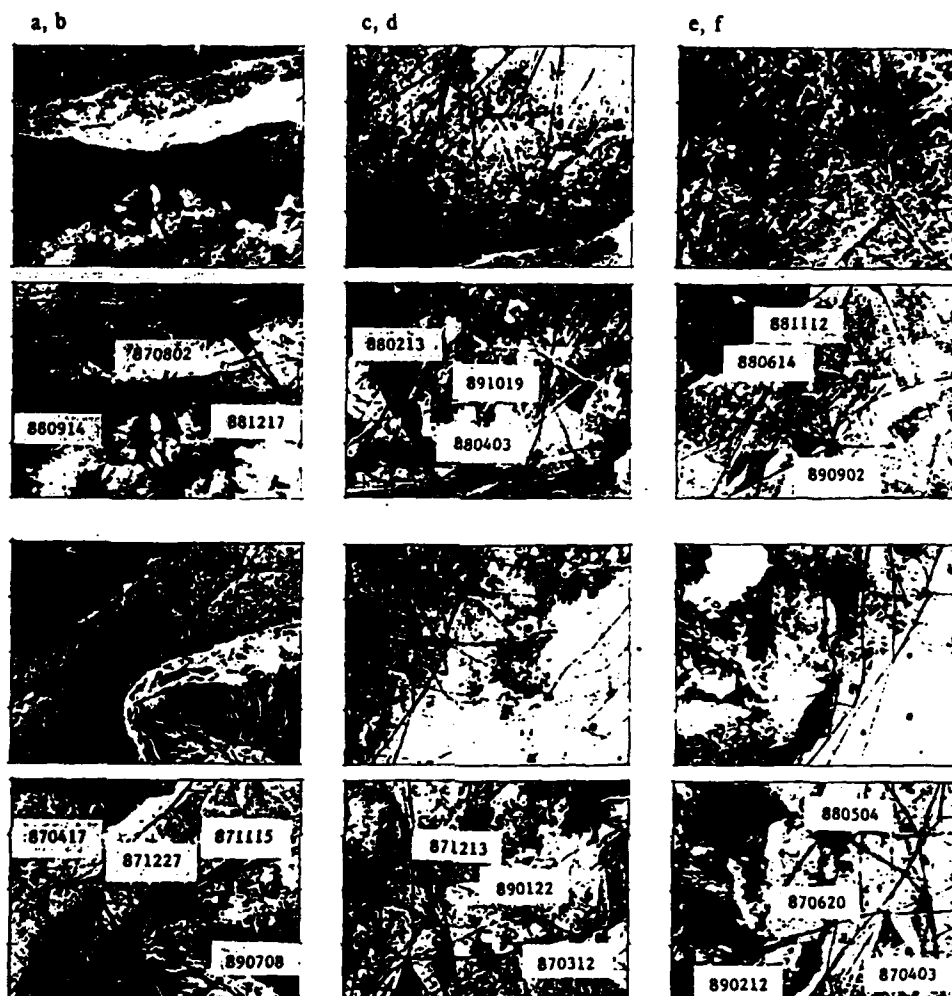Event origin times have been computed relative to that of event 99 (03 h 46 m 57.64 s) as given by Adushkin et al.

42

Fig. 2. Before-and-after SPOT images for explosion sites. Each pair shows images from 860617 (top), and 891015 (bottom) and the explosion site, as indicated below. a,b) The area of events 880914 (the JVE; above left), 870802 (below center), and 881217 (above right). c,d) The area just NE of the JVE, with events 880213 (below center), 880403 (below center), and 891019 (below center). e,f) The far NE part of Balapan, with events 880614 (below center), 881112 (above center), and 890902 (above center). g,h) The area just W of the JVE, with events 870417 (below left), 871115 (above right), 871227 (above center), and 890708 (above center). i,j) The area just N of the JVE, with events 870312 (above center), 871213 (above center), and 890122 (below center). k,l) The area NW of the JVE, with events 870403 (above center), 870620 (above center), 880504 (below center), and 890212 (above center). © 1993 CNES. Provided by SPOT Image Corporation.

(1992), keeping all epicenters and depths fixed at the values given in Table 2. The resulting values (Table 2) average 2.4 s earlier than those estimated by Lilwall and Farthing (1990).

In Figure 3, the locations derived from satellite image analysis (Table 2 and Figure 2 a-l) are compared to the JED locations (Table 1 and Figure 1). The mislocation vectors trend NNE in NE Balapan versus SSW in SW Balapan, averaging 1.2 km for the 19 unconstrained events, compared to an average error ellipse dimension of 0.7 km. The location derived from SPOT images falls within the 95% confidence ellipse for only 3 events. Doubling the size of the error ellipses increases this to 9 events. Clearly, JED seriously underestimates event mislocation. Nonuniform observation

(Pavlis, 1992), poor azimuthal coverage, and near-source velocity heterogeneity are possible causes of this discrepancy. Each could produce systematic errors that are not accounted for in the JED estimation of uncertainty, which assumes that errors are uncorrelated. These hypotheses could be tested once a larger number of accurate locations are determined

Our final event locations have value for a variety of studies. Methods for improving location and uncertainty estimates could be tested. They can be used as controlled sources for waveform modeling studies (Goldstein et al., 1992), or to improve tomographic studies of KTS (McLaughlin et al. (1992). Characteristics of the emplacement points might provide information on yield and depth of burial. The relation

43

Table 2. Locations of Balapan explosions from SPOT images

| N	YrMoDa	Hr Mn Sec	Lat (°N)	Lon (°E)
82	870312	01 57 17.2	49.9358	78.8261
83	870403	01 17 07.9	49.9186	78.7794
84	870417	01 03 04.7	49.8831	78.6708
85	870620	00 53 04.7	49.9367	78.7464
86	870802	00 58 06.8	49.8806	78.8750
87	871115	03 31 06.7	49.8981	78.7575
88	871213	03 21 04.8	49.9614	78.7933
89	871227	03 05 04.8	49.8789	78.7253
90	880213	03 05 05.8	49.9322	78.8681
91	880403	01 33 05.8	49.9069	78.9064
92	880504	00 57 06.7	49.9500	78.7494
93	880614	02 27 06.5	50.0364	78.9675
94*	880914	03 59 57.3	49.8781	78.8239
95	881112	03 30 03.8	50.0467	78.9689
96	881217	04 18 06.8	49.8797	78.9236
97	890122	03 57 06.7	49.9411	78.7869
98	890212	04 15 06.8	49.9167	78.7142
99	890708	03 46 57.6	49.8675	78.7792
100	890902	04 16 57.4	50.0094	78.9856
101	891019	09 49 57.4	49.9300	78.9456

*JVE
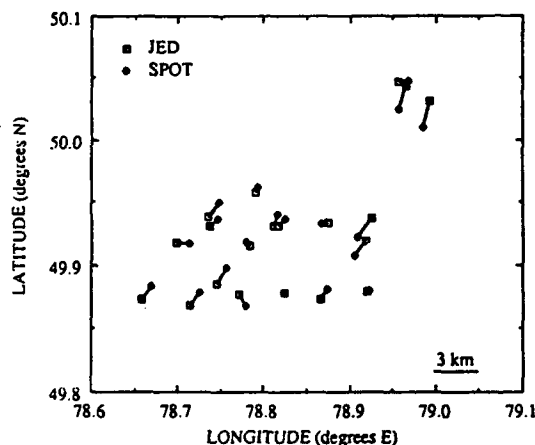
Fig. 3. Comparison of SPOT image (squares) and JED teleseismic (diamonds) locations for the recent 20 nuclear explosions at Balapan. The JVE was used as the master event. In 16 out of 19 cases, mislocations exceed the 95% confidence bounds indicated in Fig. 1.

between explosion locations and regional faults or preexisting rubble zones could provide important information for studies of tectonic release or seismic coupling. These types of analyses should prove useful for the monitoring of nuclear explosions at other historic and possibly future test sites.

References

Adushkin, V. V., A. A. Spivak, and V. I. Kulikov, Influence of tectonics and geophysical medium upon seismic waves from an underground nuclear explosion, preprint, 1992.

Bocharov, V. S., S. A. Zelentsov, and V. N. Mikhailov, Characteristics of 96 underground nuclear explosions at the Semipalatinsk test site, Atomnaya Energiya, 67, 1989.

Douglas, A., Joint epicentre determination, Nature, 215, 47-48, 1967.

Goldstein, P., W. R. Walter, and G. Zandt, Upper mantle structure beneath Central Asia using a source array of nuclear explosions and waveforms at regional distances, J. Geophys. Res., 97, 14097-14113, 1992.

Jih, R.-S., and R. A. Wagner, Recent methodological developments in magnitude determination and yield estimation with applications to Semipalatinsk explosions, PL-TR-91-2212(I), 90 pp., 1991.

Leith, W., and D. W. Simpson, Monitoring underground nuclear tests, in Commercial Observation Satellites and International Security, St. Martin's Press, NY, pp. 114-129, 1990.

Lilwall, R. C., and J. Farthing, Joint epicentre determination of Soviet underground nuclear explosions 1973-89 at the Semipalatinsk test site, Atomic Weapons Research Establishment Rept. O 12/90, 1990.

Marshall, P. D., T. C. Bache, and R. C. Lilwall, Body wave magnitudes and locations of Soviet underground explosions at the Semipalatinsk test site, Atomic Weapons Research Establishment Rept. O 16/84, 1984.

McLaughlin, K. L., J. R. Murphy, and B. W. Barker, A lithospheric velocity anomaly beneath the Shagan River test site. Part 2. Imaging and inversion with amplitude transmission tomography, Bull. Seism. Soc. Am., 82, 999-1017, 1992.

Murphy, J. R. and J. N. Jenab, Development of a comprehensive seismic yield estimation system for underground nuclear explosions, PL-TR-92-2076, 95 pp., 1992.

Pavlis, G. L., Appraising relative earthquake location errors, Bull. Seism. Soc. Am., 82, 836-859, 1992.

Ringdal, F., P. D. Marshall, and R. W. Alewine, Seismic yield determination of Soviet underground nuclear explosions at the Shagan River test site, Geophys. J. Int., 109, 65-77, 1992.

Vergino, E. S., Soviet test yields, EOS, Trans. Am. Geophys. Un., 70, 1511-1524, 1989a.

Vergino, E. S., Soviet test yields, corrections and additions, EOS, Trans. Am. Geophys. Un., 70, 1569, 1989b.

C. Thurber and H. Quin, Dept. Geology & Geophysics, UW-Madison, 1215 W. Dayton St., Madison, WI 53706.
P. Richards, Lamont-Doherty Earth Observatory, Palisades, NY 10964

2.4.4. Accurate locations of nuclear explosions at Balapan, Kazakhstan, 1973 to 1985

Introduction

Over the years 1965 through 1989, the former Soviet Union is thought to have conducted 101 nuclear tests at the Shagan River test site (Lilwall and Farthing, 1990). All of these events were recorded and located teleseismically by a large number of stations. Exact location of these events using teleseismic means alone is impossible due to the uncertainties inherent in seismic location techniques. However, in the years 1974 to 1982 the Soviet test site was imaged often by the LANDSAT satellite, and imaged frequently in the years between 1986-1989 by the SPOT satellite. These satellite images show clearly identifiable shot areas; in most cases, a circular area is visible on the satellite image at or near the junction of two or more roads. The identification of shot areas by previous work on SPOT imagery and teleseismic estimates of shot location has proven to be an effective method of obtaining exact locations of nuclear explosions for Shagan River (Thurber et al., 1993).

In this report, we present locations for suspected explosions from the Shagan River test site in the years 1965 to 1985. Starting estimates of the event locations were obtained from a revision of the results Lilwall and Farthing (1990), using the program JED, in which 27 known events were used to constrain the teleseismic locations, compared to only 7 used by Lilwall and Farthing (1990). The 7 master events used by Lilwall and Farthing (1990) are those events from the years 1965 to 1972 published by Bocharov et al. (1989). The additional 20 master events we use are those whose locations were determined from SPOT images by Thurber et al. (1993).

Using the revised location estimates, we endeavor to make accurate associations between event epicenters and identifiable shot points on rectified LANDSAT and SPOT images. The 4-band LANDSAT images are enhanced by various techniques. This enhancement allows clear identification of a large number of new shot areas occurring in a sequence of images. In this manner, stepping forward in time from image to image, overlaying shots from previous images on top of the current image, we can identify virtually all explosions occurring in the years between 1973 and 1985.

LANDSAT and SPOT Data

The images used in this study consist of a set of LANDSAT images recorded in the years 1974 to 1982. Examples are shown in Figure 7. These data are recorded at a spatial resolution of 80 meters, which was sufficient to resolve the location of the shot areas. The images were registered to a common set of ground control points obtained from a rectified SPOT 1986 image. We were able to register each of the images to within about one to two hundred meters of each

other. Each registered image covered the area between 78.6° and 79.1° E in longitude and 49.7° and 50.1° N in latitude. This covered the estimated teleseismic location of all explosions with a magnitude of about 5.0 and above at the Balapan test site.

This common rectification enabled us to make accurate comparisons of shot location between various images. By overlying the identified shot points from one image on another, we can make accurate comparisons of shot points from one year to the next. The emplacement point identifications were made on the rectified images by enhancing the images to increase the contrast of the shot points from the surrounding regions. On the enhanced images, we can make accurate picks on which shot points occurred since the last image was acquired. In this manner, proceeding forward in time image by image since 1974, by matching new emplacement locations with available teleseismic locations we can accurately identify essentially all the shot emplacement points. Our final locations are provided in Table 3, including all 101 events for convenience.

Discussion

We find that we are able to associate teleseismic shot locations with satellite images of shot points for virtually all of the shots occurring between 1973 and 1985. For most events the teleseismic locations and LANDSAT shot point estimates agree to within about 1 to 2 km. In the process of carrying out this work, we have learned that one of the events (#72 15-Sep-84) is reported by Russian scientists to be a large chemical explosion, not a nuclear explosion. This event is one of the few for which our association is uncertain. Others which we deem somewhat uncertain are indicated by an asterisk (*) in Table 3; these include events 10, 12, and 65. Event 10 is one of the smallest explosions ($m_b = 4.35$) with among the largest location uncertainties. We have associated it with an apparent cratering feature that in fact is close to (but not exactly equal to) the location given by Bocharov et al. (1990) for event 7. Thus this association is probably to be considered controversial. In the cases of events 12 and 72, the regions in which they are thought to be located (based on the teleseismic location) are quite bright and complex, so it is difficult to detect new features, especially at the low sptial resolution of the LANDSAT data. For event 65, it is quite possible that the bright feature immediately southwest of our chosen point is the explosion site, but the latter feature appears to be just a road junction, not an explosion site. Overall, the combined use of satellite imagery with teleseismic (and regional) locations should be quite useful in monitoring a global test ban for the case in which suspected test areas involve vertical drilling.

3. Conclusions and Recommendations

A plane-layered velocity model has proven adequate for waveform modeling and event location a t near-regional (< 300 km) distances in the vicinity of the Kazakhstan Test Site (KTS). We have verified that the approach of Thurber et al. (1989) and Li and Thurber (1991) of using multiple secondary body wave arrivals for event location is justified by successfully identifying and modeling Pg and PmP secondary phases, and relocating events using these confirmed phases. This approach would be practical in other areas with some calibration shot or other master event information and sparse near-regional station coverage.

For moderate regional distances (600 to 900 km), we have applied a novel modification of the generalized ray method to synthesis seismograms in a manner that accounts for differences in structure between the source region and receiver region. Models for structure beneath four Central Asia stations (BRV, FRU, NVS, and WMQ) have been derived using events from KTS and the source region structure derived above.

We give estimates, to a new level of precision, of the locations of 20 nuclear explosions at the Balapan Test Site between 1987 and 1989. We have very high confidence in the identification from SPOT images of the explosion emplacement points for 16 of the 20 explosions with $m_b > 5$ post-dating 1986. Improved temporal image coverage and/or availability of additional multispectral images from other sources might help resolve remaining uncertainties in event identification. Comparing the site locations from rectified satellite images with teleseismic joint epicenter determination (JED) results leads us to conclude that seismic epicenter uncertainties are generally underestimated by a factor of 2 or more for Shagan River. We suggest that non-uniform observation (Pavlis, 1992) combined with poor azimuthal coverage may be a major cause of this discrepancy. For the events in the time period 1973 to 1985, we have been successful in identifying explosion sites for virtually all of teleseimically-detected events, using LANDSAT and SPOT images.

Our final event locations have potential value for a variety of studies. Methods for improving location estimates and uncertainties (VanDecar and Crosson, 1990; Pavlis, 1992) could be tested with these events. They could be used as controlled sources for waveform modeling studies (Goldstein et al., 1992) and tomographic studies (McLaughlin et al., 1992). Perhaps the m_b bias variations across the Shagan River area (Ringdal et al., 1992) could be accounted for in part by lateral variations in velocity structure. The characteristics of the emplacement points might provide some information on explosion yield and depth of burial. These types of analyses could prove useful for the monitoring of explosions at other historic and possibly future test sites.

Table 3. Explosion locations from LANDSAT and SPOT images, 1973 to 1985

1	15-Jan-65	49	56	06	79	00	34
2	19-Jun-68	49	58	49	78	59	08
3	30-Nov-69	49	55	27	78	57	21
4	30-Jun-71	49	56	46	78	58	50
5	10-Feb-72	50	01	27	78	52	41
6	2-Nov-72	49	55	37	78	49	02
7	10-Dec-72	50	02	08	79	00	39
8	23-Jul-73	49	57	36	78	46	50
9	14-Dec-73	50	02	49	78	59	14
10*	16-Apr-74	50	01	37	78	59	44
11	31-May-74	49	57	46	78	51	20
12*	16-Oct-74	49	59	07	78	53	48
13	27-Dec-74	49	58	02	79	00	18
14	27-Apr-75	49	56	21	78	54	28
15	30-Jun-75	49	59	50	78	59	43
16	29-Oct-75	49	57	15	78	52	28
17	25-Dec-75	50	02	54	78	49	23
18	21-Apr-76	49	54	04	78	49	43
19	9-Jun-76	49	59	35	79	01	34
20	4-Jul-76	49	54	11	78	53	52
21	28-Aug-76	49	58	30	78	55	45
22	23-Nov-76	50	01	03	78	56	49
23	7-Dec-76	49	56	39	78	50	23
24	29-May-77	49	56	47	78	46	18
25	29-Jun-77	50	02	37	78	50	56
26	5-Sep-77	50	03	34	78	54	50
27	29-Oct-77	50	03	23	78	58	58
28	30-Nov-77	49	58	04	78	52	32
29	11-Jun-78	49	54	48	78	48	07
30	5-Jul-78	49	54	09	78	52	00
31	29-Aug-78	50	00	29	78	58	05
32	15-Sep-78	49	55	42	78	51	44
33	4-Nov-78	50	02	47	78	56	57
34	29-Nov-78	49	57	20	78	47	47
35	1-Feb-79	50	05	12	78	51	20
36	23-Jun-79	49	54	55	78	50	43
37	7-Jul-79	50	02	21	78	59	30
38	4-Aug-79	49	54	11	78	53	12
39	18-Aug-79	49	56	52	78	55	09
40	28-Oct-79	49	58	32	78	59	39
41	2-Dec-79	49	54	37	78	47	08
42	23-Dec-79	49	56	00	78	45	11
43	25-Apr-80	49	58	37	78	45	39
44	12-Jun-80	49	59	21	78	59	27
45	29-Jun-80	49	56	15	78	47	52
46	14-Sep-80	49	55	52	78	48	40
47	12-Oct-80	49	58	06	79	01	19
48	14-Dec-80	49	54	31	78	55	02
49	27-Dec-80	50	04	04	78	58	39
50	29-Mar-81	50	01	18	78	58	51
51	22-Apr-81	49	53	58	78	48	24

52	27-May-81	49	59	16	78	58	10
53	13-Sep-81	49	54	52	78	53	37
54	18-Oct-81	49	55	41	78	50	45
55	29-Nov-81	49	54	08	78	50	49
56	27-Dec-81	49	56	00	78	46	47
57	25-Apr-82	49	55	06	78	53	12
58	4-Jul-82	49	57	39	78	48	35
59	31-Aug-82	49	54	50	78	45	42
60	5-Dec-82	49	55	41	78	50	41
61	26-Dec-82	50	04	06	78	59	43
62	12-Jun-83	49	55	23	78	53	48
63	6-Oct-83	49	55	30	78	45	25
64	26-Oct-83	49	54	44	78	49	25
65*	20-Nov-83	50	04	05	79	01	03
66	19-Feb-84	49	54	01	78	44	37
67	7-Mar-84	50	03	15	78	57	16
68	29-Mar-84	49	55	21	78	55	07
69	25-Apr-84	49	56	10	78	51	05
70	26-May-84	49	58	06	79	00	13
71	14-Jul-84	49	54	27	78	52	37
72*	15-Sep-84	49	59	31	78	54	39
73	27-Oct-84	49	54	20	78	49	02
74	2-Dec-84	50	00	35	79	00	27
75	16-Dec-84	49	56	49	78	48	56
76	28-Dec-84	49	52	50	78	41	30
77	10-Feb-85	49	53	53	78	46	46
78	25-Apr-85	49	55	31	78	52	52
79	15-Jun-85	49	54	25	78	50	20
80	30-Jun-85	49	51	50	78	40	05
81	20-Jul-85	49	56	54	78	47	09
82	12-Mar-87	49	56	09	78	49	34
83	3-Apr-87	49	55	07	78	46	46
84	17-Apr-87	49	53	00	78	40	12
85	20-Jun-87	49	56	12	78	44	47
86	2-Aug-87	49	52	50	78	52	29
87	15-Nov-87	49	53	55	78	45	20
88	13-Dec-87	49	57	42	78	47	34
89	27-Dec-87	49	52	45	78	43	27
90	13-Feb-88	49	55	58	78	52	03
91	3-Apr-88	49	54	25	78	54	23
92	4-May-88	49	57	00	78	44	58
93	14-Jun-88	50	01	26	78	57	30
94	14-Sep-88	49	52	42	78	49	24
95	12-Nov-88	50	02	50	78	58	04
96	17-Dec-88	49	52	50	78	55	24
97	22-Jan-89	49	56	25	78	48	59
98	12-Feb-89	49	55	00	78	42	51
99	8-Jul-89	49	52	05	78	46	45
100	2-Sep-89	50	00	35	78	59	06
101	19-Oct-89	49	55	19	78	54	32

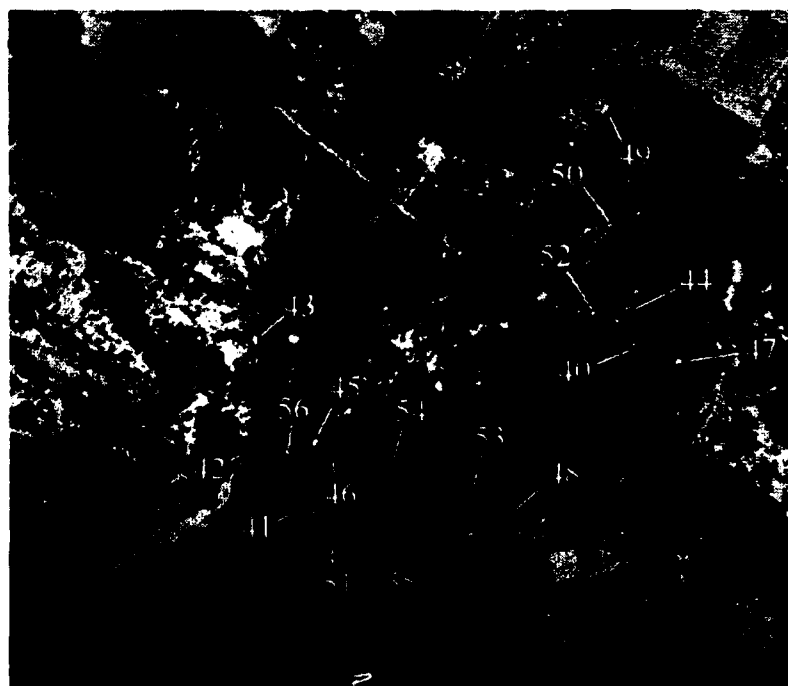* Event associations considered to be subject to some uncertainty.
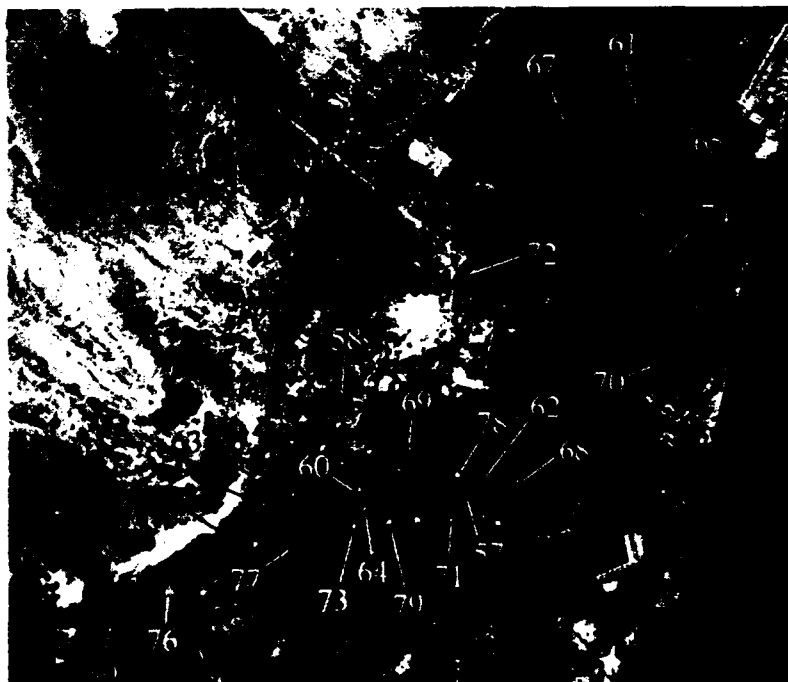
(a)

(b)

50

(c)

(d)

51
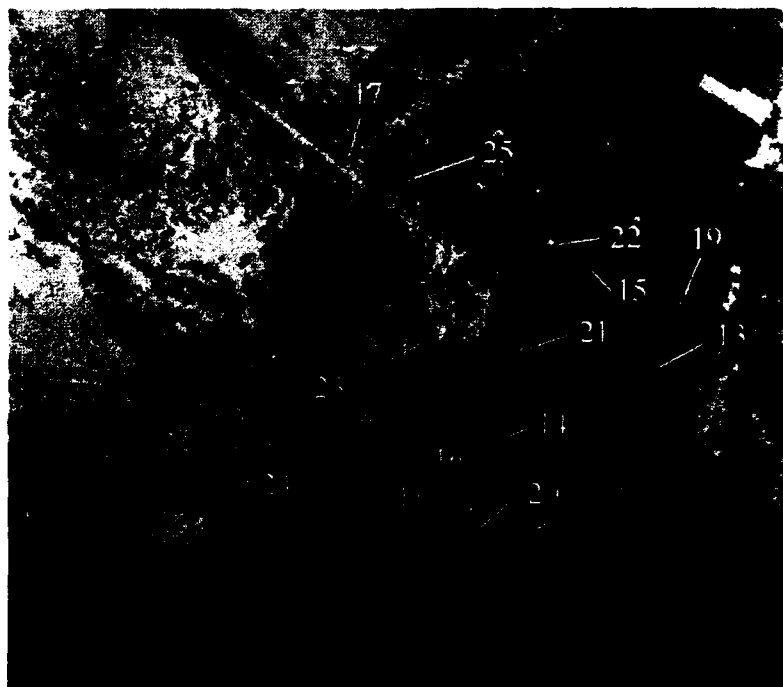
(e)

Figure 7. Examples of LANDSAT images used for identifying explosion sites, from (a) 1974, (b) 1977, (c) 1979, (d) 1981, and (e) a SPOT image from 1986 [© 1992 CNES. Provided by SPOT Image Corporation.].

4. References

Adushkin, V.V., A.A. Spivak, and V.I. Kulikov, Influence of tectonics and the geophysical medium upon seismic waves from an underground nuclear explosion, preprint, 1992.

Aki, K., and P.G. Richards, Quantitative Seismology, Theory and Methods, 932 pp., W. H. Freeman, New York, 1980.

Barker, B.W., and J.R. Murphy, A lithospheric velocity anomaly beneath the Shagan River test site. Part 1. Detection and location with network magnitude residuals, Bull. Seism. Soc. Am., 82, 980-998, 1992.

Barker, T.G., S.M. Day , A simple physical model for spall from nuclear explosions based upon two-dimensional nonlinear numerical simulations, S-Cubed Report SSS-TR-90-11550, 1990.

Barker, T.G., S.M. Day, K.L. McLaughlin, B. Shkoller, J.L. Stevens, An analysis of the effects of spall on regional and teleseismic waveforms using two-dimensional numerical modeling of underground explosions, S-Cubed Report SSS-TR-90-11536, 1990.

Berger, J., H. Eissler, F.L. Vernon, I.L. Nersesov, M.B. Gokhberg, O.A. Stolrov, and N.D. Tarassov, Studies of high-frequency seismic noise in eastern Kazakhstan, Bull. Seism. Soc. Am., 78, 1744-1758, 1988.

Bocharov, V.S., S.A. Zelentsov, and V.N. Mikhailov, Characteristics of 96 underground nuclear explosions at the Semipalatinsk test site, Atomnaya Energiya, 67, 1989.

Bratt, S.R. and T.C. Bache, Locating events with a sparse network of regional arrays, Bull. Seism. Soc. Am., 78, 780-798, 1988.

Burdick, L.J., E.J. Garnero, D.V. Helmberger and L.S. Zhao, Time domain regional discriminants, PL-TR-91-2278, 1991, ADA249949.

Day, S. M., and K.L. McLaughlin, Seismic source representation for spall, PL-TR-91-2005, 1990, ADA239064.

Douglas, A., Joint epicentre determination, Nature, 215, 47-48, 1967.

Given, H.K., N.T. Tarasov, V. Zhurravlev, F.L. Vernon, J. Berger and I.L. Nersesov, High-frequency seismic observations in eastern Kazakhstan, USSR, with emphasis on chemical explosion experiments, J. Geophys. Res., 95, 295-307, 1990.

Given, J.W. and D.V. Helmberger, Upper mantle structure of northwestern Eurasia, J. Geophys. Res., 85, 7183-7194, 1980.

Goldstein, P., W.R. Walter, and G. Zandt, Upper mantle structure beneath Central Asia using a source array of nuclear explosions and waveforms at regional distances, J. Geophys. Res., 97, 14097-14113, 1992.

Gupta , I.N., W.W. Chan, and R.A. Wagner, A comparative study of regional phases from underground nuclear explosions at East Kazakh and Nevada Test Sites, GL-TR-90-0170,

1990, ADA230567.

Jih, R.-S., and R.A. Wagner, Recent methodological developments in magnitude determination and yield estimation with applications to Semipalatinsk explosions, PL-TR-91-2212(I), 90 pp., 1991, ADA244503.

Jordan, T.H., and K.A. Sverdrup, Teleseismic location techniques and their application to earthquake clusters in the south-central Pacific, Bull. Seism. Soc. Am., 71, 1105-1130, 1981.

Jurkevics, A., Polarization analysis of three-component array data, Bull. Seism. Soc. Am., 78, 1725-1743, 1988.

Kim, W.Y. and P.G. Richards, Digital seismogram data from Borovoye Geophysical Observatory, northern Kazakhstan, IRIS DMC Dataset Report: Borovoye, 1992.

King, D.W. and G. Calcagnile, P-wave velocities in the upper mantle beneath Fennoscandia and Western Russia, Geophys. J. Roy. Astr. Soc., 46, 407-432, 1976.

Langston, C.A., Wave propagation at regional distances, PL-TR-91-2097, 1991. ADA246890

Leith, W., Geology of NRDC seismic station sites in eastern Kazakhstan, U.S.S.R., USGS Open File Rep., 87-97, 1987.

Li, Y., and C.H. Thurber, Hypocenter constraint with regional seismic data: A theoretical analysis for the Natural Resources Defense Council network in Kazakhstan, USSR, J. Geophys. Res., 96, 10,159-10,176, 1991.

Lilwall, R.C., and J. Farthing, Joint epicentre determination of Soviet underground nuclear explosions 1973-89 at the Semipalatinsk test site, AWRE Rept. O 12/90, 1990.

Magotra, N., N. Ahmed, and E.Chael, Seismic event detection and source location using single-station (three-component) data, Bull. Seism. Soc. Am., 77, 958-971, 1987.

Mangino, S. and J. Ebel, The receiver structure beneath the Chinese Digital Seismograph Network (CDSN) stations, unpublished manuscript, 1992.

Marshall, P.D., T.C. Bache, and R.C. Lilwall, Body wave magnitudes and locations of Soviet underground explosions at the Semipalatinsk test site, AWRE Rept. O 16/84, 1984.

McLaughlin, K.L., T.G. Barker, S.M. Day, B Shkoller , J.L. Stevens, Effects of depth of burial and tectonic strain release on regional and teleseismic explosion waveforms, AFGL-TR-88-0314, 1988, ADA207541.

McLaughlin, K.L., J.R. Murphy, and B.W. Barker, A lithospheric velocity anomaly beneath the Shagan River test site. Part 2. Imaging and inversion with amplitude transmission tomography, Bull. Seism. Soc. Am., 82, 999-1017, 1992.

Murphy, J.R. and J.N. Jenab, Development of a comprehensive seismic yield estimation system for underground nuclear explosions, PL-TR-92-2076, 95 pp., 1992, ADA254346.

Murphy, J. R., J.L. Stevens, D.C. O'Neill, B.W. Barker, K.L. McLaughlin, and M.E. Marshall,

Development of a comprehensive seismic yield estimation system for underground nuclear explosions, PL-TR-91-2161, 36 pp., 1991, ADA240814.

Oreshin, S., G. Kosarev, N. Petersen and L.P. Vinnik, Deep structure underneath seismograph station Borovoye, EOS. Trans. Am. Geophys. Un., 73, 209, 1992.

Pavlenkova, N.I. and A.V. Yegorkin, Upper mantle heterogeneity in the northern part of Eurasia, Phys. Earth Planet. Int., 33, 180-193, 1983.

Pavlis, G.L., Appraising relative earthquake location errors, Bull. Seism. Soc. Am., 82, 836-859, 1992.

Priestly, K.F., G. Zandt, and G.E. Randall, Crustal structure in eastern Kazakh, USSR, from teleseismic receiver functions, Geophys. Res. Lett., 15, 613-616, 1988.

Ringdal, F., P.D. Marshall, and R.W. Alewine, Seismic yield determination of Soviet underground nuclear explosions at the Shagan River test site, Geophys. J. Int., 109, 65-77, 1992.

Riviere-Barbier, F., A. Suteau-Henson, V.Z. Ryaboy, and J.A. Carter, Analysis of 3-component data from IRIS/IDA stations in the USSR, Bull. Seism. Soc. Am., 192-220, 1992.

Ryaboy, V.Z., Upper mantle structure studies by explosion seismology in the U.S.S.R., DELPHIC Associates, Arlington VA, 154 pp., 1990.

Saika, C.K. and L.J. Burdick, Fine structure of P_{nl} waves from explosions, J. Geophys. Res, 96, 14,383-14,401, 96, 1991.

Sereno, T.J., Frequency-dependent attenuation in eastern Kazakhstan and implications for seismic detection thresholds in the Soviet Union, Bull. Seism. Soc. Am., 80, 2089-2105, 1990.

Thurber, C.H., Analysis methods for kinematic data from local earthquakes, Rev. Geophys., 24, 793-805, 1986.

Thurber, C., H. Given, and J. Berger, Regional seismic event location with a sparse network: application to eastern Kazakhstan, USSR, J. Geophys. Res., 92, 17767-780, 1989.

Thurber, C.H., H.R. Quin and P.G. Richards, Accurate locations of nuclear explosions in Balapan, Kazakhstan, 1987 to 1989, Geophys. Res. Lett., 5, 399-402, 1993.

VanDecar, J.C. and R.S. Crosson, Determination of teleseismic relative phase arrival times using multi-channel cross correlation and least squares, Bull. Seism. Soc. Am., 80, 150-169, 1990.

Vergino, E.S., Soviet test yields, EOS. Trans. Am. Geophys. Un., 70, 1511-1524, 1989a.

Vergino, E.S., Soviet test yields, corrections and additions, EOS. Trans. Am. Geophys. Un., 70, 1569, 1989b.

Wu, Francis T., Studies of regional phases and discriminants in Asia, GL-TR-90-0017, 1991, ADA222184.

Prof. Thomas Ahrens
Seismological Lab, 252-21
Division of Geological & Planetary Sciences
California Institute of Technology
Pasadena, CA 91125

Prof. Keiiti Aki
Center for Earth Sciences
University of Southern California
University Park
Los Angeles, CA 90089-0741

Prof. Shelton Alexander
Geosciences Department
403 Deike Building
The Pennsylvania State University
University Park, PA 16802

Dr. Ralph Alewine, III
DARPA/NMRO
3701 North Fairfax Drive
Arlington, VA 22203-1714

Prof. Charles B. Archambeau
CIRES
University of Colorado
Boulder, CO 80309

Dr. Thomas C. Bache, Jr.
Science Applications Int'l Corp.
10260 Campus Point Drive
San Diego, CA 92121 (2 copies)

Prof. Muawia Barazangi
Institute for the Study of the Continent
Cornell University
Ithaca, NY 14853

Dr. Jeff Barker
Department of Geological Sciences
State University of New York
 at Binghamton
Vestal, NY 13901

Dr. Douglas R. Baumgardt
ENSCO, Inc
5400 Port Royal Road
Springfield, VA 22151-2388

Dr. Susan Beck
Department of Geosciences
Building #77
University of Arizona
Tuscon, AZ 85721

Dr. T.J. Bennett
S-CUBED
A Division of Maxwell Laboratories
11800 Sunrise Valley Drive, Suite 1212
Reston, VA 22091

Dr. Robert Blandford
AFTAC/TT, Center for Seismic Studies
1300 North 17th Street
Suite 1450
Arlington, VA 22209-2308

Dr. Stephen Bratt
Center for Seismic Studies
1300 North 17th Street
Suite 1450
Arlington, VA 22209-2308

Dr. Lawrence Burdick
Woodward-Clyde Consultants
566 El Dorado Street
Pasadena, CA 91109-3245

Dr. Robert Burridge
Schlumberger-Doll Research Center
Old Quarry Road
Ridgefield, CT 06877

Dr. Jerry Carter
Center for Seismic Studies
1300 North 17th Street
Suite 1450
Arlington, VA 22209-2308

Dr. Eric Chael
Division 9241
Sandia Laboratory
Albuquerque, NM 87185

Dr. Martin Chapman
Department of Geological Sciences
Virginia Polytechnical Institute
21044 Derring Hall
Blacksburg, VA 24061

Prof. Vernon F. Cormier
Department of Geology & Geophysics
U-45, Room 207
University of Connecticut
Storrs, CT 06268

Prof. Steven Day
Department of Geological Sciences
San Diego State University
San Diego, CA 92182

Marvin Denny
U.S. Department of Energy
Office of Arms Control
Washington, DC 20585

Dr. Zoltan Der
ENSCO, Inc.
5400 Port Royal Road
Springfield, VA 22151-2388

Prof. Adam Dziewonski
Hoffman Laboratory, Harvard University
Dept. of Earth Atmos. & Planetary Sciences
20 Oxford Street
Cambridge, MA 02138

Prof. John Ebel
Department of Geology & Geophysics
Boston College
Chestnut Hill, MA 02167

Eric Fielding
SNEE Hall
INSTOC
Cornell University
Ithaca, NY 14853

Dr. Mark D. Fisk
Mission Research Corporation
735 State Street
P.O. Drawer 719
Santa Barbara, CA 93102

Prof Stanley Flatte
Applied Sciences Building
University of California, Santa Cruz
Santa Cruz, CA 95064

Dr. John Foley
NER-Geo Sciences
1100 Crown Colony Drive
Quincy, MA 02169

Prof. Donald Forsyth
Department of Geological Sciences
Brown University
Providence, RI 02912

Dr. Art Frankel
U.S. Geological Survey
922 National Center
Reston, VA 22092

Dr. Cliff Frolich
Institute of Geophysics
8701 North Mopac
Austin, TX 78759

Dr. Holly Given
IGPP, A-025
Scripps Institute of Oceanography
University of California, San Diego
La Jolla, CA 92093

Dr. Jeffrey W. Given
SAIC
10260 Campus Point Drive
San Diego, CA 92121

Dr. Dale Glover
Defense Intelligence Agency
ATTN: ODT-1B
Washington, DC 20301

Dr. Indra Gupta
Teledyne Geotech
314 Montgomery Street
Alexanderia, VA 22314

Dan N. Hagedon
Pacific Northwest Laboratories
Battelle Boulevard
Richland, WA 99352

Dr. James Hannon
Lawrence Livermore National Laboratory
P.O. Box 808
L-205
Livermore, CA 94550

Dr. Roger Hansen
HQ AFTAC/TTR
Patrick AFB, FL 32925-6001

Prof. David G. Harkrider
Seismological Laboratory
Division of Geological & Planetary Sciences
California Institute of Technology
Pasadena, CA 91125

Prof. Danny Harvey
CIRES
University of Colorado
Boulder, CO 80309

3

Dr. Gary McCartor
Department of Physics
Southern Methodist University
Dallas, TX 75275

Dr. Bao Nguyen
HQ AFTAC/TTR
Patrick AFB, FL 32925-6001

Prof. Thomas V. McEvilly
Seismographic Station
University of California
Berkeley, CA 94720

Prof. John A. Orcutt
IGPP, A-025
Scripps Institute of Oceanography
University of California, San Diego
La Jolla, CA 92093

Dr. Art McGarr
U.S. Geological Survey
Mail Stop 977
U.S. Geological Survey
Menlo Park, CA 94025

Prof. Jeffrey Park
Kline Geology Laboratory
P.O. Box 6666
New Haven, CT 06511-8130

Dr. Keith L. McLaughlin
S-CUBED
A Division of Maxwell Laboratory
P.O. Box 1620
La Jolla, CA 92038-1620

Dr. Howard Patton
Lawrence Livermore National Laboratory
L-025
P.O. Box 808
Livermore, CA 94550

Stephen Miller & Dr. Alexander Florence
SRI International
333 Ravenswood Avenue
Box AF 116
Menlo Park, CA 94025-3493

Dr. Frank Pilotte
HQ AFTAC/TT
Patrick AFB, FL 32925-6001

Prof. Bernard Minster
IGPP, A-025
Scripps Institute of Oceanography
University of California, San Diego
La Jolla, CA 92093

Dr. Jay J. Pulli
Radix Systems, Inc.
2 Taft Court, Suite 203
Rockville, MD 20850

Prof. Brian J. Mitchell
Department of Earth & Atmospheric Sciences
St. Louis University
St. Louis, MO 63156

Dr. Robert Reinke
ATTN: FCTVTD
Field Command
Defense Nuclear Agency
Kirtland AFB, NM 87115

Mr. Jack Murphy
S-CUBED
A Division of Maxwell Laboratory
11800 Sunrise Valley Drive, Suite 1212
Reston, VA 22091 (2 Copies)

Prof. Paul G. Richards
Lamont-Doherty Geological Observatory
 of Columbia University
Palisades, NY 10964

Dr. Keith K. Nakanishi
Lawrence Livermore National Laboratory
L-025
P.O. Box 808
Livermore, CA 94550

Mr. Wilmer Rivers
Teledyne Geotech
314 Montgomery Street
Alexandria, VA 22314

Dr. Carl Newton
Los Alamos National Laboratory
P.O. Box 1663
Mail Stop C335, Group ESS-3
Los Alamos, NM 87545

Dr. George Rothe
HQ AFTAC/TTR
Patrick AFB, FL 32925-6001

4

Dr. Alan S. Ryall, Jr.
DARPA/NMRO
3701 North Fairfax Drive
Arlington. VA 22209-1714

Dr. Richard Sailor
TASC, Inc.
55 Walkers Brook Drive
Reading, MA 01867

Prof. Charles G. Sammis
Center for Earth Sciences
University of Southern California
University Park
Los Angeles, CA 90089-0741

Prof. Christopher H. Scholz
Lamont-Doherty Geological Observatory
of Columbia University
Palisades, NY 10964

Dr. Susan Schwartz
Institute of Tectonics
1156 High Street
Santa Cruz, CA 95064

Secretary of the Air Force
(SAFRD)
Washington, DC 20330

Office of the Secretary of Defense
DDR&E
Washington, DC 20330

Thomas J. Sereno, Jr.
Science Application Int'l Corp.
10260 Campus Point Drive
San Diego, CA 92121

Dr. Michael Shore
Defense Nuclear Agency/SPSS
6801 Telegraph Road
Alexandria, VA 22310

Dr. Robert Shumway
University of California Davis
Division of Statistics
Davis, CA 95616

Dr. Matthew Sibol
Virginia Tech
Seismological Observatory
4044 Derring Hall
Blacksburg, VA 24061-0420

Prof. David G. Simpson
IRIS, Inc.
1616 North Fort Myer Drive
Suite 1440
Arlington, VA 22209

Donald L. Springer
Lawrence Livermore National Laboratory
L-025
P.O. Box 808
Livermore, CA 94550

Dr. Jeffrey Stevens
S-CUBED
A Division of Maxwell Laboratory
P.O. Box 1620
La Jolla, CA 92038-1620

Lt. Col. Jim Stobie
ATTN: AFOSR/NL
Bolling AFB
Washington, DC 20332-6448

Prof. Brian Stump
Institute for the Study of Earth & Man
Geophysical Laboratory
Southern Methodist University
Dallas, TX 75275

Prof. Jeremiah Sullivan
University of Illinois at Urbana-Champaign
Department of Physics
1110 West Green Street
Urbana, IL 61801

Prof. L. Sykes
Lamont-Doherty Geological Observatory
of Columbia University
Palisades, NY 10964

Dr. David Taylor
ENSCO, Inc.
445 Pineda Court
Melbourne, FL 32940

Dr. Steven R. Taylor
Los Alamos National Laboratory
P.O. Box 1663
Mail Stop C335
Los Alamos, NM 87545

Prof. Clifford Thurber
University of Wisconsin-Madison
Department of Geology & Geophysics
1215 West Dayton Street
Madison, WS 53706

DARPA/PM
3701 North Fairfax Drive
Arlington, VA 22203-1714

Prof. M. Nafi Toksoz
Earth Resources Lab
Massachusetts Institute of Technology
42 Carleton Street
Cambridge, MA 02142

DARPA/RMO/RETRIEVAL
3701 North Fairfax Drive
Arlington, VA 22203-1714

Dr. Larry Turnbull
CIA-OSWR/NED
Washington, DC 20505

DARPA/RMO/SECURITY OFFICE
3701 North Fairfax Drive
Arlington, VA 22203-1714

Dr. Gregory van der Vink
IRIS, Inc.
1616 North Fort Myer Drive
Suite 1050
Arlington, VA 22209

HQ DNA
ATTN: Technical Library
Washington, DC 20305

Dr. Karl Veith
EG&G
5211 Auth Road
Suite 240
Suitland, MD 20746

Defense Intelligence Agency
Directorate for Scientific & Technical Intelligence
ATTN: DTIB
Washington, DC 20340-6158

Prof. Terry C. Wallace
Department of Geosciences
Building #77
University of Arizona
Tuscon, AZ 85721

Defense Technical Information Center
Cameron Station
Alexandria, VA 22314 (2 Copies)

Dr. Thomas Weaver
Los Alamos National Laboratory
P.O. Box 1663
Mail Stop C335
Los Alamos, NM 87545

TACTEC
Battelle Memorial Institute
505 King Avenue
Columbus, OH 43201 (Final Report)

Dr. William Wortman
Mission Research Corporation
8560 Cinderbed Road
Suite 700
Newington, VA 22122

Phillips Laboratory
ATTN: XPG
Hanscom AFB, MA 01731-5000

Prof. Francis T. Wu
Department of Geological Sciences
State University of New York
at Binghamton
Vestal, NY 13901

Phillips Laboratory
ATTN: GPE
Hanscom AFB, MA 01731-5000

AFTAC/CA
(STINFO)
Patrick AFB, FL 32925-6001

Phillips Laboratory
ATTN: TSML
Hanscom AFB, MA 01731-5000

6

Phillips Laboratory
ATTN: SUL
Kirtland, NM 87117 (2 copies)

Dr. Svein Mykkeltveit
NTNT/NORSAR
P.O. Box 51
N-2007 Kjeller, NORWAY (3 Copies)

Dr. Michel Bouchon
I.R.I.G.M.-B.P. 68
38402 St. Martin D'Heres
Cedex, FRANCE

Prof. Keith Priestley
University of Cambridge
Bullard Labs, Dept. of Earth Sciences
Madingley Rise, Madingley Road
Cambridge CB3 OEZ, ENGLAND

Dr. Michel Campillo
Observatoire de Grenoble
I.R.I.G.M.-B.P. 53
38041 Grenoble, FRANCE

Dr. Jorg Schlittenhardt
Federal Institute for Geosciences & Nat'l Res.
Postfach 510153
D-3000 Hannover 51, GERMANY

Dr. Kin Yip Chun
Geophysics Division
Physics Department
University of Toronto
Ontario, CANADA

Dr. Johannes Schweitzer
Institute of Geophysics
Ruhr University/Bochum
P.O. Box 1102148
4360 Bochum 1, GERMANY

Prof. Hans-Peter Harjes
Institute for Geophysic
Ruhr University/Bochum
P.O. Box 102148
4630 Bochum 1, GERMANY

Trust & Verify
VERTIC
8 John Adam Street
LONDON WC2N 6EZ, ENGLAND

Prof. Eystein Husebye
NTNF/NORSAR
P.O. Box 51
N-2007 Kjeller, NORWAY

David Jepsen
Acting Head, Nuclear Monitoring Section
Bureau of Mineral Resources
Geology and Geophysics
G.P.O. Box 378, Canberra, AUSTRALIA

Ms. Eva Johannisson
Senior Research Officer
FOA
S-172 90 Sundbyberg, SWEDEN

Dr. Peter Marshall
Procurement Executive
Ministry of Defense
Blacknest, Brimpton
Reading FG7-FRS, UNITED KINGDOM

Dr. Bernard Massinon, Dr. Pierre Mechler
Societe Radiomana
27 rue Claude Bernard
75005 Paris, FRANCE (2 Copies)